Multistart spiral electron vortices in ionization by circularly polarized UV pulses

J. M. Ngoko Djiokap,[1] A. V. Meremianin,[2] N. L. Manakov,[2] S. X. Hu,[3] L. B. Madsen,[4] and Anthony F. Starace[1]

[1]*Department of Physics and Astronomy, University of Nebraska, Lincoln, Nebraska 68588-0299, USA*

[2]*Department of Physics, Voronezh State University, Voronezh 394006, Russia*

[3]*Laboratory for Laser Energetics, University of Rochester, Rochester, New York 14623-1299, USA*

[4]*Department of Physics and Astronomy, Aarhus University, DK-8000 Aarhus C, Denmark*

(Received 18 April 2016; published 12 July 2016)

Multistart spiral vortex patterns are predicted for the electron momentum distributions in the polarization plane following ionization of the helium atom by two time-delayed circularly polarized ultrashort laser pulses. For two ultraviolet (UV) pulses having the same frequency (such that two photons are required for ionization), single-color two-photon interferometry with corotating or counter-rotating time-delayed pulses is found to lead respectively to *zero*-start or *four*-start spiral vortex patterns in the ionized electron momentum distributions in the polarization plane. In contrast, two-color one-photon plus two-photon interferometry with time-delayed corotating or counter-rotating UV pulses is found to lead respectively to *one*-start or *three*-start spiral vortex patterns. These predicted *multistart* electron vortex patterns are found to be sensitive to the carrier frequencies, handedness, time delay, and relative phase of the two pulses. Our numerical predictions are obtained by solving the six-dimensional two-electron time-dependent Schrödinger equation (TDSE). They are explained analytically using perturbation theory (PT). Comparison of our TDSE and PT results for single-color two-photon processes probes the role played by the time-delay-dependent ionization cross channels in which one photon is absorbed from each pulse. Control of these cross channels by means of the parameters of the fields and the ionized electron detection geometries is discussed.

DOI: 10.1103/PhysRevA.94.013408

I. INTRODUCTION

Wave-particle duality [1] is one of the most fundamental aspects of quantum mechanics. Whereas the photoelectric effect [2] introduced firm evidence of the particle nature of light, the de Broglie hypothesis [1] and the subsequent electron-diffraction experiments of Davisson and Germer [3] established the wave nature of the electron. Dramatic evidence of the wavelike nature of the electron has been provided by the experimental observation of Ramsey interference [4] of laser-produced electron wave packets in both Rydberg states [5,6] and in the continuum [7] using linearly polarized lasers.

Recently an unusual kind of Ramsey interference between continuum photoelectron wave packets was predicted [8]. It was found that when the helium atom is ionized by a pair of time-delayed oppositely circularly polarized attosecond laser pulses, the photoelectron wave packets produced by each pulse interfere in such a way that the photoelectron momentum distribution forms a *two*-start Fermat spiral vortex pattern. Moreover the matter-wave (electron) vortices predicted in Ref. [8] have a counterpart in optics: in Ref. [9] similar vortex patterns were produced by superposing two optical vortex beams having opposite helicities and different wave-front curvatures, with each beam having an orbital angular momentum of unity (the first-order 01^* doughnut mode). In addition, *four*- and *six*-start spirals were also observed by interfering optical beams of opposite helicities having orbital angular momenta of 2 (the 02^* mode) and 3 (the 03^* mode), respectively [9]. While *even*-start spiral vortices were thus observed optically [9], *odd*-start optical vortices were not reported. We note also that photoelectron momentum distributions following strong-field ionization of Ar (in the tunneling regime) [10] and ionization of H (in the multiphoton regime) [11] by corotating or counter-rotating two-color circularly polarized fields were found to exhibit single-lobe or three-lobe structures, respectively. Spiral vortex patterns, however, were not reported in Refs. [10,11].

In this paper we predict both analytically and numerically the occurrence of higher order *even*-start and *odd*-start spiral vortices. These vortices occur in the polarization plane momentum distributions of electrons ionized from the helium atom by two time-delayed, ultrashort, circularly polarized laser pulses having either the same or opposite helicities. The higher order *even*-start spiral vortices are produced by single-color two-photon interferometry [cf. Fig. 1(a)] while the *odd*-start spiral vortices are produced by two-color one-photon plus two-photon interferometry [cf. Fig. 1(b)]. The intensities of our ultraviolet (UV) laser pulses are such that all processes take place in the perturbative multiphoton regime. We analyze the cases of both corotating and counter-rotating circularly polarized time-delayed UV pulses. The ionized electron momentum distributions are obtained by solving numerically the six-dimensional two-electron time-dependent Schrödinger equation (TDSE). Perturbation theory (PT) is used to analyze the patterns exhibited by the momentum distributions. Within our PT formalism, a connection between our electron matter-wave vortices and vortices in a physical process associated with zeros in the scattering wave function [12–20] has been established [8]. In contrast to *dynamical* vortex patterns, which depend upon the transition amplitudes of the process considered, the vortex patterns in the ionized electron momentum distributions we predict here (and in Ref. [8]) stem from the ionized electron detection geometry. They are thus *kinematical* vortex patterns. Moreover, our predicted *four*-start electron matter-wave vortices correspond to the optical ones found in Ref. [9], providing thus another example of wave-particle duality. Also, our *odd*-start vortices are consistent with recent strong-field [10] and multiphoton [11] results.

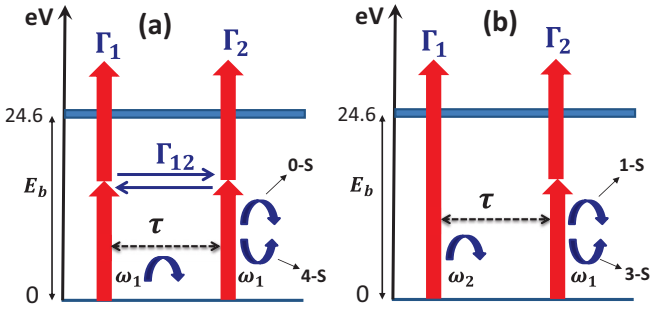

FIG. 1. Schematic energy-level diagrams for the cases of single ionization of He (with binding energy $E_b = 24.6$ eV) by two circularly polarized pulses delayed in time by τ that are considered in this paper: (a) Two-photon interferometry for a carrier frequency $\omega_1 = 15$ eV, which leads to either *zero*-start (0-S) or *four*-start (4-S) vortex patterns for equal or opposite helicity pulses; and (b) two-color interferometry for carrier frequencies $\omega_2 = 2\omega_1 = 30$ eV, which leads to either *one*-start (1-S) or *three*-start (3-S) vortex patterns for equal or opposite helicity pulses. In each case, the ionization pathways Γ_1, Γ_{12} and/or Γ_2 are shown.

Two-photon interferometry has recently been used as a tool for investigation of various atomic photoionization processes [21–23]. In Refs. [21,22], double ionization of the helium atom by a pair of time-delayed extreme UV pulses by means of several different pathways was investigated. In contrast to the present case of single ionization of He, the photon energy $\hbar\omega$ in each of Refs. [21,22] was always greater than the He binding energy, $E_b = 24.6$ eV. In Ref. [23], two-pathway interference between a fundamental UV pulse and its second harmonic with zero time delay between the pulses was recently used to predict forward-backward asymmetries in the photoelectron angular distributions for the H atom. In all these interferometry studies the two pulses were linearly polarized.

The two circularly polarized pulse interferometric cases we investigate in this paper for single ionization of He are shown schematically in Fig. 1. The single-color two-photon interferometric case is shown in Fig. 1(a), which indicates that there are three pathways: Path Γ_1 indicates single ionization of He by two-photon absorption from the first pulse; path Γ_2 indicates single ionization by two-photon absorption from the second pulse; and path Γ_{12} indicates the cross path in which single ionization occurs by absorption of one photon from each of the two pulses, possibly with different helicities. For illustrative purposes, Fig. 1(a) shows that the first pulse is right circularly polarized, while the second pulse (delayed in time by τ) can be either right or left circularly polarized. As explained in Sec. IV below, in the former case the ionized electron momentum distribution in the polarization plane is not spiral and is designated as "zero-start" (or "0-S"), while in the latter case we predict a four-start Fermat spiral vortex pattern (or "4-S"). The two-color one-photon plus two-photon interferometric case is shown in Fig. 1(b), which indicates that there are only two paths: Path Γ_1 indicates in this case single ionization of He by absorption of a second harmonic photon from the first pulse, and path Γ_2 indicates single ionization by absorption of two fundamental photons from the second pulse. As explained in Sec. V below, if the time-delayed circularly polarized pulses have the same handedness, the ionized electron momentum distribution in the polarization plane exhibits a one-start Fermat spiral pattern (or "1-S"), while if the pulses have opposite handedness a three-start Fermat spiral pattern (or "3-S") is realized.

This paper is organized as followed. In Sec. II, we describe briefly our computational methods. In Sec. III, we provide some general considerations governing the requirements for observing electron matter-wave vortices. In Secs. IV and V we present our PT analyses and our numerical results for the processes in Figs. 1(a) and 1(b) respectively. In Sec. VI we summarize our results and present some conclusions. In Appendix A, we present a derivation of our PT parametrization of the second-order amplitude for single ionization of an s-electron in an atom such as He by a pair of arbitrarily polarized pulses. In Appendix B we describe our procedure for determining from our TDSE results a key scalar dynamical parameter on which our PT formulas depend. Atomic units (a.u.) are used throughout this paper unless specified otherwise.

II. COMPUTATIONAL METHOD

To demonstrate numerically *multistart* spiral vortex patterns in photoelectron momentum distributions for the illustrative case of He, we solve the six-dimensional two-electron TDSE for the He atom interacting with a pair of circularly polarized pulses. Within the length gauge and the dipole approximation, the TDSE is

$$i\partial_t \Psi(\mathbf{r}_1,\mathbf{r}_2,t) = \left[-\frac{1}{2}(\Delta_{\mathbf{r}_1}+\Delta_{\mathbf{r}_1}) - \frac{2}{\mathbf{r}_1} - \frac{2}{\mathbf{r}_2} + \frac{1}{|\mathbf{r}_1-\mathbf{r}_2|} + \mathbf{F}(t)\cdot(\mathbf{r}_1+\mathbf{r}_2)\right]\Psi(\mathbf{r}_1,\mathbf{r}_2,t), \quad (1)$$

where $\mathbf{r}_1$ and $\mathbf{r}_2$ are the spatial coordinates of the two electrons, and $\mathbf{F}(t)$ is the electric field of our pair of pulses delayed in time by τ,

$$\begin{aligned}\mathbf{F}(t) &= \mathbf{F}_1(t) + \mathbf{F}_2(t-\tau) \\ &\equiv F_0^{(1)}(t)\,\mathrm{Re}\,[\mathbf{e}_1 e^{-i(\omega^{(1)}t+\phi_1)}] \\ &\quad + F_0^{(2)}(t-\tau)\,\mathrm{Re}\,[\mathbf{e}_2 e^{-i[\omega^{(2)}(t-\tau)+\phi_2]}]. \end{aligned} \quad (2)$$

For the jth pulse ($j = 1,2$) in Eq. (2), $\omega^{(j)}$ is its carrier frequency [which can take the values $\omega_1 = 15$ eV or $\omega_2 = 2\omega_1 = 30$ eV depending on the process considered; see Figs. 1(a) and 1(b)]; $\mathbf{e}_j$ is its polarization vector ($\mathbf{e}_j \cdot \mathbf{e}_j^* = 1$); ϕ_j is its carrier envelope phase (CEP); and $F_0^{(j)}(t) = F_0^{(j)}\cos^2(\pi t/T_j)$ is its smooth temporal envelope (with $F_0^{(j)}$ the electric field amplitude), for which $-T_j/2 \leqslant t \leqslant T_j/2$, where $T_j = N_j(2\pi/\omega_j)$ gives its total pulse duration, with N_j being the number of optical cycles. It is useful to parametrize the polarization vector of the jth pulse as

$$\mathbf{e}_j \equiv (\hat{\boldsymbol{\epsilon}} + i\eta_j\hat{\boldsymbol{\xi}})/\sqrt{1+\eta_j^2}, \quad (3)$$

where η_j is the ellipticity ($-1 \leqslant \eta_j \leqslant +1$), $\hat{\boldsymbol{\epsilon}}$ and $\hat{\boldsymbol{\xi}} \equiv \hat{\mathbf{k}} \times \hat{\boldsymbol{\epsilon}}$ are respectively the major and minor axes of the polarization ellipse, and $\hat{\boldsymbol{k}} \parallel \hat{\mathbf{z}}$ is the pulse propagation direction. For the jth pulse, the degrees of linear and circular polarization are respectively $\ell_j \equiv (\mathbf{e}_j \cdot \mathbf{e}_j) = (1-\eta_j^2)/(1+\eta_j^2)$ and $\xi_j \equiv$

$\mathrm{Im}\,[\mathbf{e}_j^* \times \mathbf{e}_j]_z = 2\eta_j/(1+\eta_j^2)$, where $\ell_j^2 + \xi_j^2 = 1$. Finally, the laser field $\mathbf{F}(t)$ in Eq. (2) turns on at $t = T_i = -T_1/2$ and ends at $t = T_f = \tau + T_2/2$.

To obtain the wave packet $\Psi(\mathbf{r}_1,\mathbf{r}_2,t)$ solution of the TDSE (1), we use the methods developed previously for either an arbitrarily polarized attosecond single pulse [24] or a pair of pulses [8]. In brief, we adopt the time-dependent close-coupling expansion [25,26] of the wave packet $\Psi(\mathbf{r}_1,\mathbf{r}_2,t)$ onto the orthonormal basis functions of bipolar spherical harmonics $\Lambda_{l_1,l_2}^{LM_L}(\hat{\mathbf{r}}_1,\hat{\mathbf{r}}_2)$, where L is the total angular momentum of the two-electron system, M_L is its azimuthal quantum number, and l_1,l_2 are the individual electron orbital angular momenta. For ionization of the He atom interacting with a linearly polarized pulse, one has $[H,L_z] = 0$, so that the magnetic quantum number M_L is conserved. Parity is also a good quantum number. Thus, for the interaction of the $^1\mathrm{S}^e$ ground state (having $M_L = 0$) with linearly polarized photons, M_L is unchanged during the time propagation, reducing thus the numerical complexity of the problem.

In contrast, for pulses with nonzero ellipticity, $[H,L_z] \neq 0$, so that M_L is not conserved, thus giving rise to the so-called M_L-mixing problem [27,28]. To overcome this problem, we adopt the basic ideas and principles of the method introduced in Ref. [27] and developed intensively in Refs. [28–33]. It consists of the introduction of a rotational transformation between two frames: (i) the atomic fixed frame in the laboratory coordinate system and (ii) the rotating frame defined by the external pulse polarization vector. The latter frame is rotated with respect to the laboratory frame by the Euler angles (α,β,γ) by using the Wigner rotation operator $D(\alpha,\beta,\gamma)$, whose matrix elements are

$$\langle L' M'_{L'}|D(\alpha,\beta,\gamma)|L M_L\rangle = e^{iM'_{L'}\alpha} d^L_{M'_{L'},M_L}(-\beta) e^{iM_L\gamma}\delta_{LL'}, \quad (4)$$

which is diagonal in L but not in M_L. Thus the matrix $d^L_{M_L,M'_{L'}}(\beta)$ is block diagonal within the L representation. We then use the finite-element discrete-variable representation combined with the real-space-product algorithm (a split-operator method) [34] as well as Wigner rotation transformations at each time step from the laboratory frame to the frame of the instantaneous electric field [27,28]. The key consequence of this procedure [27,28] is that the electric field seen by an observer in the rotating frame is always linearly polarized, so that treating the laser-atom interaction in the rotating frame simplifies its calculation. Moreover, this procedure is quite accurate as long as the time step is sufficiently small, which we ensure in all our numerical TDSE calculations.

At the end of the two pulses, i.e., at $t = T_f$, we extract the triply differential probability (TDP) [35] for single ionization of He to $\mathrm{He}^+(1s)$ from the wave packet $\Psi(\mathbf{r}_1,\mathbf{r}_2,t)$ by projecting it onto correlated field-free Jacobi matrix wave functions $\Theta^{(-)}_{1s,\mathbf{p}}(\mathbf{r}_1,\mathbf{r}_2)$ [36]. The TDP, $d^3W/d^3\mathbf{p} \equiv \mathcal{W}^{\xi_1}_{\xi_2}(\mathbf{p})$, for single electron ionization to the continuum with momentum $\mathbf{p} \equiv (p,\theta,\varphi)$ is thus

$$\frac{d^3W}{d^3\mathbf{p}} \equiv \left|\left\langle \Theta^{(-)}_{1s,\mathbf{p}}(\mathbf{r}_1,\mathbf{r}_2)\middle|\Psi\left(\mathbf{r}_1,\mathbf{r}_2,\mathbf{e}_{\phi_1},\mathbf{e}_{\phi_2},T_f\right)\right\rangle\right|^2, \quad (5)$$

where $\mathbf{e}_{\phi_j} \equiv \mathbf{e}_j e^{-i\phi_j}$, with $j = 1,2$. We include four total angular momenta ($L = 0$–3), their azimuthal quantum numbers $|M_L| \leqslant L$, all combinations of individual electron orbital angular momenta $l_1,l_2 = 0$–5, and their azimuthal quantum numbers $|m_1| \leqslant l_1$ and $|m_2| \leqslant l_2$.

III. GENERAL CONSIDERATIONS

As the electron vortices we predict (for single ionization of He by a pair of circularly polarized pulses, delayed in time by τ) are essentially perturbative effects, their observation requires that the laser pulse parameters are such that PT is applicable [37]. For the laser frequencies we employ (see below) and for experimentally accessible intensities below 10^{14} W/cm^2, this is the case. Moreover, for these laser parameters the rotating wave approximation (RWA) is valid, i.e., it is legitimate to neglect photon emission processes in our PT analysis.

Experimental observation of the multistart spiral electron vortices we predict requires the large bandwidth $\Delta\omega$ characteristic of ultrashort pulses, as the bandwidth must support several spiral fringes [8], i.e., $2\pi/\tau < \Delta\omega$. However, the carrier frequency, peak intensity, and spectral width of each pulse must be chosen such that single ionization of He by a single pulse is possible via either *only* one-photon absorption or *only* two-photon absorption. This requires a pulse bandwidth that is not too large. The binding energy of the He atom in its ground state is $E_b = 24.6$ eV.

Choosing a laser pulse with an intensity of 1 TW/cm^2 (i.e., 10^{12} W/cm^2) and a carrier frequency ω_2 greater than E_b (e.g., $\omega_2 = 30$ eV) should thus result in single-photon ionization, which according to PT must scale linearly with intensity. Likewise, for such weak peak pulse intensities, a carrier frequency ω_1 smaller than E_b, but with $2\omega_1 > E_b$ should result in two-photon ionization, which according to PT must scale quadratically with intensity. The latter expectation holds only when the pulse bandwidth $\Delta\omega_1$ does not favor single-photon single ionization. This is guaranteed when using a pulse having more than $N = 5$ optical cycles within its cosine squared envelope. Throughout this work, for a carrier frequency $\omega_1 = 15$ eV we choose $N = 6$ optical cycles (to avoid populating singly excited states by one-photon transitions), which gives a pulse bandwidth of $\Delta\omega_1 = 1.44\omega_1/N = 3.6$ eV. For all these processes, our pulse intensities are too weak to induce higher-order nonlinear effects. Our focus is thus on the photoelectron energy spectrum ($0 \leqslant E \leqslant 15$ eV) around the first above threshold ionization peak.

The TDP for ionization of He leading to an electron in the continuum with momentum $\mathbf{p}$ with the residual ion being in its ground state $\mathrm{He}^+(1s)$ is

$$\frac{d^3W}{d^3\mathbf{p}} \equiv \mathcal{W}^{\xi_1}_{\xi_2}(\mathbf{p}) = \mathcal{C}\left|A^{\xi_1}_{\xi_2}(\mathbf{p})\right|^2, \quad (6)$$

where $A^{\xi_1}_{\xi_2}(\mathbf{p})$ is the PT ionization amplitude for our pair of pulses, and $\mathcal{C}$ is a normalization factor independent of the electron momentum $\mathbf{p}$. In Secs. IV and V below, we parametrize the transition amplitudes $A^{\xi_1}_{\xi_2}(\mathbf{p})$ for the $(2\omega_1 + 2\omega_1)$ and the $(\omega_2 + 2\omega_1)$ ionization processes in Figs. 1(a) and 1(b) respectively. For each process, we present our analytic PT and numerical TDSE results for the cases in which the two pulses are circularly polarized in the same direction, $\mathbf{e}_1 = \mathbf{e}_2$ (i.e., $\xi_1 = \xi_2 = \xi$), or in opposite directions, $\mathbf{e}_1 =$

$\mathbf{e}_2^*$, (i.e., $\xi_1 = -\xi_2 = \pm 1$). For the single-color two-photon process [Fig. 1(a)], electric dipole selection rules for the final state (i.e., $L = 0,2$ and $M_L = \pm 2,0$) produced by oppositely circularly polarized pulses differ from those [i.e., $L = 2, M_L = +2\,(-2)$] produced respectively by two identical right (left) circularly polarized pulses. For the two-color one-photon plus two-photon process [Fig. 1(b)], the electric dipole selection rules for the final state give $L = 1,2$ with $M_L = \pm 1, \pm 2$, where the sign $+\,(-)$ corresponds respectively to a right (left) circularly polarized pulse.

IV. SINGLE-COLOR TWO-PHOTON SINGLE IONIZATION OF HELIUM BY A PAIR OF CIRCULARLY POLARIZED PULSES

The second-order amplitude for single ionization of an s electron in the ground state of an atom (with energy E_i) by two-photon absorption from a pair of arbitrarily polarized pulses, delayed in time by τ, can be parametrized as follows (see Appendix A for the derivation):

$$\begin{aligned} A_{\xi_2}^{\xi_1}(\mathbf{p}) = e^{-2i\phi_1}\{&\big[\mathcal{M}_d^{(1)}(p)(\hat{\mathbf{p}}\cdot\mathbf{e}_1)^2 + \ell_1\mathcal{M}_{ds}^{(1)}(p)\big] \\ &+ e^{2i\psi}\big[\mathcal{M}_d^{(2)}(p)(\hat{\mathbf{p}}\cdot\mathbf{e}_2)^2 + \ell_2\mathcal{M}_{ds}^{(2)}(p)\big] \\ &+ e^{i\psi}\big[\mathcal{M}_d^{(12)}(p,\tau)(\hat{\mathbf{p}}\cdot\mathbf{e}_1)(\hat{\mathbf{p}}\cdot\mathbf{e}_2) \\ &+ \mathcal{M}_{ds}^{(12)}(p,\tau)(\mathbf{e}_1\cdot\mathbf{e}_2)\big]\}, \end{aligned} \tag{7}$$

where ℓ_j, the linear polarization degree for the jth pulse, $j = 1,2$, is defined below Eq. (3). In accord with our PT assumption in Sec. III, we have ignored photon emission terms. In Eq. (7), the τ-dependent phase ψ is

$$\psi = \omega\tau + \phi_{12}, \tag{8}$$

where $\phi_{12} \equiv \phi_1 - \phi_2$ is the relative CEP and $\omega \equiv \omega_1$ throughout this section. The τ-independent dynamical radial parameter $\mathcal{M}_d^{(1)}(p) \equiv \mathcal{M}_d^{(1)}$ in Eq. (7) corresponds to a transition to a final D state:

$$\begin{aligned} \mathcal{M}_d^{(1)} = \frac{\sqrt{2}i}{4(2\pi)^{3/2}}\frac{e^{i\delta_2}}{p}\int_{-\infty}^{\infty}\hat{F}_0(\epsilon)\,\hat{F}_0(\omega_{fi} - 2\omega - \epsilon) \\ \times\langle p2|dg_1(E_f - \omega - \epsilon)d'|n_i0\rangle\,d\epsilon, \end{aligned} \tag{9}$$

where $\mathbf{d}$ is the electric dipole moment operator of the two electrons, and $\omega_{fi} \equiv E_f - E_i$, where E_f is the final-state energy of the two-electron system. For single electron ionization of the He ground state, $\omega_{fi} = E + E_b$, where $E = p^2/2$ is the photoelectron kinetic energy and $E_b \equiv E_{1s} - E_i = 0.9037$ a.u. is the ground-state binding energy. In Eq. (9) (and in equations below), we employ a simplified notation for the antisymmetrized two-electron states in which we indicate explicitly only the state of the active electron and suppress that of the spectator electron in the He $1s$ state; see Appendix A for a more detailed discussion of our notation. Thus, $|nl\rangle$ and $|pl'\rangle$ define the bound and continuum states of the active electron respectively (with n indicating the principal quantum number of the intermediate state, p indicating the ionized electron's momentum, and l and l' indicating the orbital angular momenta); $|n_i0\rangle$ is the initial state of the active electron. The continuum states have momentum normalization, i.e., $\langle pl'|p'l'\rangle = \delta(p - p')$. In Eq. (9), the superscript (1) indicates that both photons are absorbed from the first pulse; δ_l is the lth partial phase shift; $g_l(\epsilon)$ is the two-electron radial Green function,

$$g_l(\epsilon) = \sum_{n\neq n_i}\frac{|nl\rangle\langle nl|}{E_{nl} - \epsilon + i0}, \tag{10}$$

where E_{nl} is the energy associated with the intermediate state $|nlm\rangle$; and $\hat{F}_0$ is the Fourier transform of the envelope function

$$\hat{F}_0(\epsilon) = \int_{-\infty}^{\infty}F_0(t)\,e^{i\epsilon t}dt. \tag{11}$$

Likewise, the τ-independent dynamical radial parameter $\mathcal{M}_s^{(1)}(p) \equiv \mathcal{M}_s^{(1)}$ corresponds to a transition to a final S state:

$$\begin{aligned} \mathcal{M}_s^{(1)} = -\frac{\sqrt{2}i}{6(4\pi)^{3/2}}\frac{e^{i\delta_0}}{p}\int_{-\infty}^{\infty}\hat{F}_0(\epsilon)\,\hat{F}_0(\omega_{fi} - 2\omega - \epsilon) \\ \times\langle p0|dg_1(E_f - \omega - \epsilon)d'|n_i0\rangle\,d\epsilon. \end{aligned} \tag{12}$$

The parameter $\mathcal{M}_{ds}^{(1)}(p)$ in Eq. (7) is defined by

$$\mathcal{M}_{ds}^{(1)}(p) = \mathcal{M}_s^{(1)}(p) - \tfrac{1}{3}\mathcal{M}_d^{(1)}(p). \tag{13}$$

Note that the entire contribution of $\mathcal{M}_s^{(1)}$ to Eq. (7) is contained in the dynamical parameter $\mathcal{M}_{ds}^{(1)}(p) \equiv \mathcal{M}_{ds}^{(1)}$.

The corresponding τ-independent dynamical parameters $\mathcal{M}_d^{(2)}$ and $\mathcal{M}_{ds}^{(2)}$ for the second pulse differ from $\mathcal{M}_d^{(1)}$ and $\mathcal{M}_{ds}^{(1)}$ for the first pulse by only a time-delay dependent phase factor [see Eq. (A12)],

$$\mathcal{M}_{d,ds}^{(2)} = e^{i(\omega_{fi}-2\omega)\tau}\mathcal{M}_{d,ds}^{(1)} \equiv e^{i(\omega_{fi}-2\omega)\tau}\mathcal{M}_{d,ds}. \tag{14}$$

The τ-dependent parameters $\mathcal{M}_{d,ds}^{(12)}(p,\tau) \equiv \mathcal{M}_{d,ds}^{(12)}$ in Eq. (7) correspond to the two cross channels in which photons are absorbed from different pulses. The dynamical parameters $\mathcal{M}_d^{(12)}(p,\tau)$ leading to final D states are

$$\begin{aligned} \mathcal{M}_d^{(12)}(p,\tau) = \frac{\sqrt{2}i}{4(2\pi)^{3/2}}\frac{e^{i\delta_2}}{p}\int_{-\infty}^{\infty}\mathcal{F}(\epsilon,\tau) \\ \times\langle p2|dg_1(E_f - \omega - \epsilon)d'|n_i0\rangle d\epsilon \end{aligned} \tag{15}$$

and the dynamical parameters $\mathcal{M}_s^{(12)}(p,\tau)$ leading to final S states are

$$\begin{aligned} \mathcal{M}_s^{(12)}(p,\tau) = -\frac{\sqrt{2}i}{6(4\pi)^{3/2}}\frac{e^{i\delta_0}}{p}\int_{-\infty}^{\infty}\mathcal{F}(\epsilon,\tau) \\ \times\langle p0|dg_1(E_f - \omega - \epsilon)d'|n_i0\rangle d\epsilon. \end{aligned} \tag{16}$$

Finally, the parameters $\mathcal{M}_{ds}^{(12)}(p,\tau)$ are defined by

$$\mathcal{M}_{ds}^{(12)}(p,\tau) = \mathcal{M}_s^{(12)}(p,\tau) - \tfrac{1}{3}\mathcal{M}_d^{(12)}(p,\tau). \tag{17}$$

The τ dependence of the cross channel parameters in Eqs. (15)–(17) enters explicitly through the function

$$\begin{aligned} \mathcal{F}(\epsilon,\tau) = 2e^{i(\omega_{fi}/2-\omega)\tau}\hat{F}_0(\epsilon)\hat{F}_0(\omega_{fi} - 2\omega - \epsilon) \\ \times\cos[(\epsilon + \omega - \omega_{fi}/2)\tau], \end{aligned} \tag{18}$$

which oscillates rapidly as τ increases. This behavior of the function $\mathcal{F}(\epsilon,\tau)$ kills the contribution of the ionization cross channel parameters (15) and (17), i.e., they only contribute in cases of short pulse delays.

Using Eq. (14), the second-order PT amplitude (7) takes the form

$$A_{\xi_2}^{\xi_1}(\mathbf{p}) = e^{-2i\phi_1}\{\mathcal{M}_d(p)[(\hat{\mathbf{p}}\cdot\mathbf{e}_1)^2 + e^{i\Phi}(\hat{\mathbf{p}}\cdot\mathbf{e}_2)^2] + \mathcal{M}_{ds}(p)(\ell_1 + e^{i\Phi}\ell_2) + e^{i\psi}[\mathcal{M}_d^{(12)}(p,\tau)(\hat{\mathbf{p}}\cdot\mathbf{e}_1)(\hat{\mathbf{p}}\cdot\mathbf{e}_2) + \mathcal{M}_{ds}^{(12)}(p,\tau)(\mathbf{e}_1\cdot\mathbf{e}_2)]\}, \quad (19)$$

where the relative phase

$$\Phi = (E + E_b)\tau + 2(\phi_1 - \phi_2) \equiv (p^2/2 + E_b)\tau + 2\phi_{12} \quad (20)$$

is comprised of two terms: $(E + E_b)\tau$, the difference in the phase accumulation during the temporal evolution of the two electronic wave packets produced by the pathways Γ_1 and Γ_2 [cf. Fig. 1(a)], and $2\phi_{12}$, twice the relative CEP. Clearly all these dynamical parameters [in Eqs. (9), (13), and (14)–(17)] scale linearly with the peak pulse intensity. In what follows, we investigate, first, the case of a pair of identical circularly polarized pulses and, second, the case of oppositely circularly polarized pulses.

A. Two-photon single ionization by two identical, time-delayed circularly polarized pulses, including pulse overlap effects

For two identical circularly polarized pulses, $\mathbf{e}_1 = \mathbf{e}_2 = \mathbf{e}$, $\ell_1 = \ell_2 = \ell = 0$, and $\xi_1 = \xi_2 = \xi = \pm 1$. Thus, from Eq. (3) and PT formula (19) the second-order PT amplitude $A_\xi^\xi(\mathbf{p})$ for single ionization by our two identical pulses is

$$A_\xi^\xi(\mathbf{p}) = e^{-2i\phi_1}(\mathbf{e}\cdot\hat{\mathbf{p}})^2[\mathcal{M}_d(1 + e^{i\Phi}) + e^{i\psi}\mathcal{M}_d^{(12)}], \quad (21)$$

where the geometric factor $(\mathbf{e}\cdot\hat{\mathbf{p}})^2$ is

$$(\mathbf{e}\cdot\hat{\mathbf{p}})^2 = \tfrac{1}{2}\sin^2\theta e^{\pm 2i\varphi} \equiv \sqrt{8\pi/15}Y_{2,M_L}(\theta,\varphi), \quad (22)$$

with the azimuthal quantum number $M_L = +2$ (-2) for right (left) circular polarization; $\mathcal{M}_d^{(1)}(p) \equiv \mathcal{M}_d(p)$ corresponds to the path Γ_1 [cf. Fig. 1(a)] that describes two-photon absorption from the first pulse; $\mathcal{M}_d^{(2)}(p) \simeq \mathcal{M}_d^{(1)}(p)$ corresponds to the path Γ_2 [cf. Fig. 1(a)] that describes two-photon absorption from the second pulse, which is delayed by a time τ relative to the first pulse; and $\mathcal{M}_d^{(12)}(p,\tau) \equiv \mathcal{M}_d^{(12)}$ corresponds to the two pathways Γ_{12} [cf. Fig. 1(a)] that describe one-photon absorption from each pulse (in the case that the pulses overlap). Clearly, the geometric factor (22) shows that all four pathways lead to the same final state, defined by $L = 2$ with $M_L = +2$ $(M_L = -2)$ for right (left) circularly polarized pulses respectively.

Substituting Eqs. (21) and (22) into Eq. (6), the TDP for single ionization by two identical circularly polarized pulses becomes explicitly

$$\mathcal{W}_\xi^\xi(\mathbf{p}) = \frac{\mathcal{C}}{2}\Big\{2|\mathcal{M}_d(p)|^2\cos^2(\Phi/2) + \frac{1}{2}\big|\mathcal{M}_d^{(12)}(p,\tau)\big|^2 + \mathrm{Re}\big[\mathcal{M}_d^*(p)\mathcal{M}_d^{(12)}(p,\tau)\big][\cos\psi + \cos(\psi - \Phi)] + \mathrm{Im}\big[\mathcal{M}_d^*(p)\mathcal{M}_d^{(12)}(p,\tau)\big] \times [\sin\psi + \sin(\psi - \Phi)]\Big\}\sin^4\theta. \quad (23)$$

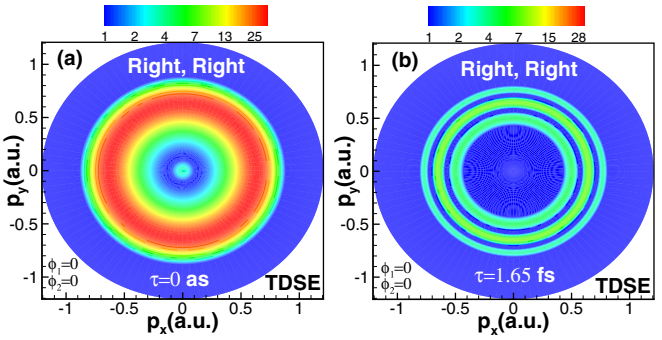

FIG. 2. Triply differential probability (TDP) $d^3W/d^3\mathbf{p}$ [see Eqs. (5), (23), (8), and (20)] in the polarization plane for single ionization of He by two right circularly polarized pulses delayed in time by (a) $\tau = 0$, and (b) $\tau = 1.65$ fs. Each cosine-squared pulse has a carrier frequency $\omega_1 = 15$ eV, $N = 6$ optical cycles, total duration $T = 1.65$ fs, and peak intensity $I = 10^{12}$ W/cm^2. The CEPs are $\phi_1 = 0$ and $\phi_2 = 0$. The magnitudes of the TDPs (in units of 10^{-7} a.u.) are indicated by the color scales in (a) and (b).

Note that only the dynamical parameter $\mathcal{M}_d^{(12)}(p,\tau)$ (15) depends on the time delay. Also, while all dynamical parameters in Eq. (23) depend upon the electron energy, $E = p^2/2$, they are independent of the momentum direction, $\hat{\mathbf{p}}$, and the pulse parameters $\mathbf{e}_1$, $\mathbf{e}_2$, and ϕ_{12}. Consequently, the TDP (23) is independent of φ and its polar angle plots in the polarization plane ($\theta = \pi/2$) have circularly symmetric patterns, as shown in Fig. 2 for momentum distributions (obtained by *ab initio* TDSE calculations) produced by two right circularly polarized six-cycle pulses with zero CEPs for two time delays: $\tau = 0$ and $\tau = 1.65$ fs. Owing to the τ and p dependence of the relative phase Φ [cf. Eq. (20)] and the τ dependence of the phase ψ [cf. Eq. (8)], for $\tau = 0$ there is no structure in the momentum distribution [cf. Fig. 2(a)]. For $\tau = T = 1.65$ fs, however, the contributions of the ionization cross channels Γ_{12} are already negligible according to our discussion following PT formula (18). Hence, Ramsey interference of the electronic wave packets produced by transitions Γ_1 and Γ_2 has a form similar to Newton's rings, i.e., bright and dark fringes along the radial direction in momentum space. The interference pattern in Fig. 2(b) is similar to that found in interference of two identical optical beams [9]. The *zero*-start circularly symmetric patterns, or Newton's rings, in Figs. 2(a) and 2(b) are also similar to the photoelectron momentum distributions produced by single-photon ionization of He by two identical circularly polarized attosecond pulses [8].

For a quantitative comparison, numerical results using PT formula (23) can also be obtained. This requires accurate dynamical parameters $\mathcal{M}_d(p)$ [see Eq. (9)] and $\mathcal{M}_d^{(12)}(p,\tau)$ [see Eq. (15)]. Analytical calculations of $\mathcal{M}_d(p)$ and $\mathcal{M}_d^{(12)}(p,\tau)$ are nontrivial as they involve Green's functions and summations over the energies of intermediate states. The parameter $\mathcal{M}_d(p)$ can be extracted numerically by means of *ab initio* TDSE calculations for a *single* right circularly polarized pulse that includes only the $L = 2, M_L = +2$ amplitude (see Appendix B). The dynamical parameter $\mathcal{M}_d^{(12)}(p,\tau)$ cannot be obtained that way as its calculation requires two pulses. However, for zero time delay between the two pulses, the

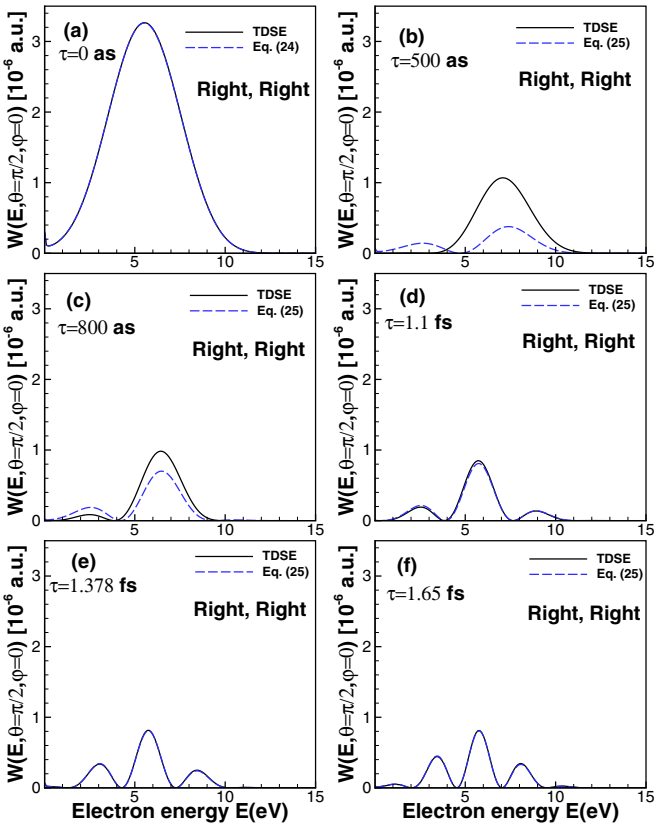

FIG. 3. Energy distributions in the polarization plane for electrons ejected at the angle $\varphi = 0$ following two-photon single ionization of He by two right circularly polarized pulses delayed in time by (a) $\tau = 0$, (b) $\tau = 500$ as, (c) $\tau = 800$ as, (d) $\tau = 1.102$ fs, (e) $\tau = 1.378$ fs, and (f) $\tau = 1.654$ fs. Results are obtained by *ab initio* TDSE calculations using Eq. (5). For comparison, we also show results using PT formula (24) [see panel (a)] or (25) [see panels (b)–(f)], in which the dynamical parameter $\mathcal{M}_d(p)$ is extracted numerically from *ab initio* TDSE calculations for a *single* pulse including *only* the $L = 2, M_L = +2$ amplitude; see Appendix B. The pulse parameters are the same as in Fig. 2.

dynamical parameter $\mathcal{M}_d^{(12)}(p,0)$ [see Eqs. (15) and (18)] is twice that of the dynamical parameter $\mathcal{M}_d(p)$. Hence, for $\tau = 0$ and $\phi_{12} = 0$ as in Figs. 2(a) and 3(a), the TDP using PT formula (23) reduces to

$$\mathcal{W}_\xi^\xi(p,\theta,\varphi) = 4\mathcal{C}|\mathcal{M}_d(p)|^2 \sin^4\theta. \tag{24}$$

Thus, when the two pulses have zero time delay, the momentum distributions [see Fig. 2(a)], the energy distributions [see Fig. 3(a)], and the angular distributions (not shown) from either a TDSE calculation or by using the PT formula (24) are in excellent quantitative agreement.

According to our discussion following PT formula (18), for time delays τ equal to or longer than the total pulse duration T, the TDP reduces to the following form:

$$\mathcal{W}_\xi^\xi(p,\theta,\varphi) = \mathcal{C}|\mathcal{M}_d(p)|^2 \sin^4\theta \cos^2(\Phi/2). \tag{25}$$

Equation (25) excludes contributions from the ionization cross channels Γ_{12}. It should nevertheless provide accurate results for the TDP because when the two pulses do not overlap, the cross channel transitions cannot take place. This PT prediction is confirmed in Fig. 3(f) in which results for the ionized electron energy distributions calculated by solving the TDSE or by using PT formula (25) are shown to coincide.

For time delays $\tau < T$ in which the two pulses overlap in time, the ionization cross channels can play a significant role. However, owing to the cosine term in Eq. (18), PT predicts that their contribution to the TDP decreases as the time delay increases. It is useful to define a critical time delay τ_c beyond which the cross channels do not contribute to TDP. For the case of $N = 6$ optical cycles, Figs. 3(b)–3(e) show energy distributions for four time delays τ shorter than the total pulse duration $T = 1.65$ fs. One sees that results obtained by solving the TDSE and by using PT formula (25) coincide for 1.1 fs $\leqslant \tau < T$ [see Figs. 3(d) and 3(e)] but differ for $0 < \tau < 1.1$ fs [see Figs. 3(b) and 3(c)]. The discrepancies for shorter time delays are due to the ionization cross channels that are taken into account in the TDSE results. Thus, for this case, $\tau_c = 1.1$ fs.

The τ-dependent ionization cross channels are also sensitive to the bandwidth of the pulses. For $N = 5$ optical cycles, which corresponds to a pulse bandwidth of $\Delta\omega_1 = 4.3$ eV and a total pulse duration of $T = 1.378$ fs, the critical time delay beyond which the ionization cross channels Γ_{12} do not contribute significantly to the TDP is once again $\tau_c \simeq 1.1$ fs, as found in Fig. 3 for $N = 6$ optical cycles. However, for $N = 7$ optical cycles, which corresponds to a smaller pulse bandwidth of $\Delta\omega_1 = 3.08$ eV and a total pulse duration of $T = 1.93$ fs, the critical time delay is $\tau_c = 1.378$ fs. Moreover, the critical time delay τ_c appears to be insensitive to the relative CEP $\phi_{12} = \phi_1 - \phi_2$ of the two pulses. Specifically, for our six-cycle pair of pulses, we carried out numerical calculations for $\phi_{12} = 0$ and $\phi_{12} = \pi/2$ (not shown) and found that the critical time delay τ_c was the same for both cases. These results indicate that the CEP-invariant effect of the ionization cross channels on the TDP can provide precise information on the overlap of the two pulses.

For longer time delays $\tau \geqslant \tau_c$, the energy spectra displayed in Figs. 3(d)–3(f) permit one to directly measure the time delay between the two pulses by measuring the energy separation between two consecutive dark (interference minimum) or bright (interference maximum) fringes. According to the PT analysis, this difference equals $2\pi/\tau$ owing to the dependence of the TDP (25) on the phase Φ (20).

B. Single-color two-photon single ionization by two oppositely circularly polarized pulses, including pulse overlap effects

For two oppositely circularly polarized pulses, $\mathbf{e}_1^* = \mathbf{e}_2$, $\ell_1 = \ell_2 = 0$, and $\xi_1 = -\xi_2 = \pm 1$. The PT amplitude $A_{\xi_2}^{\xi_1}(\mathbf{p})$ in Eq. (19) for single ionization by two oppositely circularly polarized pulses delayed in time by τ is

$$A_{\xi_2}^{\xi_1}(\mathbf{p}) = e^{-2i\phi_1}\{\mathcal{M}_d(p)[(\hat{\mathbf{p}}\cdot\mathbf{e}_1)^2 + e^{i\Phi}(\hat{\mathbf{p}}\cdot\mathbf{e}_2)^2] + e^{i\psi}\left[\mathcal{M}_d^{(12)}(p,\tau)|\hat{\mathbf{p}}\cdot\mathbf{e}_1|^2 + \mathcal{M}_{ds}^{(12)}(p,\tau)\right]\}, \tag{26}$$

where the geometric factor $|\hat{\mathbf{p}}\cdot\mathbf{e}_1|^2$ is

$$|\mathbf{e}_1\cdot\hat{\mathbf{p}}|^2 = \tfrac{1}{2}\sin^2\theta = \tfrac{1}{6}[2 - \sqrt{16\pi/5}Y_{2,0}(\theta,\varphi)]. \tag{27}$$

From the geometric factor $(\mathbf{e}\cdot\hat{\mathbf{p}})^2$ (22), where $\mathbf{e} = \mathbf{e}_1, \mathbf{e}_2$, one sees that the ionization channel $\Gamma_1(\Gamma_2)$ for the first (second)

pulse is described by the parameter $\mathcal{M}_d(p)$ [$\mathcal{M}_d^{(2)}(p) \simeq \mathcal{M}_d(p)$]. These channels lead to final states defined by $L = 2$ with $M_L^{\Gamma_1} = -M_L^{\Gamma_2} = \pm 2$, where + (−) indicates right (left) circular polarization. According to the geometric factor $|\mathbf{e}_1 \cdot \hat{\mathbf{p}}|^2$ (27), the cross channels $\mathcal{M}_d^{(12)}(p,\tau)$ correspond to transitions to final states with $L = 2$, $M_L = 0$. Finally, $\mathcal{M}_{ds}^{(12)}(p,\tau)$ in Eq. (26) describes transitions to final states with $L = 0,2$, $M_L = 0$.

Using Eqs. (6) and (26) together with the geometric factors (22) and (27), the TDP for a pair of oppositely circularly polarized pulses takes the form

$$\begin{aligned}\mathcal{W}_{\xi_2}^{\xi_1}(\mathbf{p}) = \mathcal{C}\{&|\mathcal{M}_d(p)|^2 \sin^4\theta \cos^2(\Phi/2 - 2\xi_1\varphi) \\ &+ |\Gamma^{(12)}(p,\theta,\tau)|^2 + |\mathcal{M}_d^*(p)\Gamma^{(12)}(p,\theta,\tau)| \sin^2\theta \\ &\times [\cos(\Theta + \psi - 2\xi_1\varphi) \\ &+ \cos(\Theta + \psi + 2\xi_1\varphi + \Phi)]\}, \end{aligned} \tag{28}$$

where $\xi_1 = -\xi_2 = \pm 1$ corresponds to a right and left (+) or a left and right (−) circularly polarized pair of pulses. Note that the first term in Eq. (28) results from the squared modulus of the sum of the first term (path Γ_1) and the second term (path Γ_2) in Eq. (26). In the TDP (28), the newly introduced dynamical parameter $\Gamma^{(12)}(p,\theta,\tau)$ associated with the paths Γ_{12} is defined as

$$\Gamma^{(12)}(p,\theta,\tau) \equiv \mathcal{M}_d^{(12)}(p,\tau)|\hat{\mathbf{p}} \cdot \mathbf{e}_1|^2 + \mathcal{M}_{ds}^{(12)}(p,\tau), \tag{29}$$

and the ϕ_{12}-independent dynamical angle $\Theta(p,\theta,\tau)$ (which depends upon the photoelectron energy $E = p^2/2$, its polar angle θ, and the time delay τ) is defined as

$$\tan\Theta(p,\theta,\tau) = \frac{\mathrm{Im}\,[\mathcal{M}_d^*(p)\Gamma^{(12)}(p,\theta,\tau)]}{\mathrm{Re}\,[\mathcal{M}_d^*(p)\Gamma^{(12)}(p,\theta,\tau)]}. \tag{30}$$

Perturbatively, the TDP (28) is expected to be dominated by the amplitudes for the paths Γ_1 and Γ_2. This contribution, denoted by $\mathcal{W}_{\xi_2}^{\xi_1(\Gamma_1,\Gamma_2)}(\mathbf{p})$, is given by the first term in the TDP (28):

$$\mathcal{W}_{\xi_2}^{\xi_1(\Gamma_1,\Gamma_2)}(\mathbf{p}) = \mathcal{C}|\mathcal{M}_d(p)|^2 \sin^4\theta \cos^2(\Phi/2 - 2\xi_1\varphi). \tag{31}$$

In the polarization plane ($\theta = \pi/2$), the leading term (31) of the TDP (28) has the form of a *four*-start spiral structure, as can be seen from the following considerations. The leading term, $\mathcal{W}_{\xi_2}^{\xi_1(\Gamma_1,\Gamma_2)}(\mathbf{p})$ (31), is maximal for $\Phi/2 - 2\xi_1\varphi = \Phi/2 + 2\xi_2\varphi = \pi n$ and zero for $\Phi/2 - 2\xi_1\varphi = \Phi/2 + 2\xi_2\varphi = (2n+1)\pi/2$, where $n = 0, \pm 1, \pm 2 \ldots$, and $0 \leqslant \varphi \leqslant 2\pi$. Using Eq. (20), the p dependencies of the polar angles φ at these maximum and zero values of $\mathcal{W}_{\xi_2}^{\xi_1(\Gamma_1,\Gamma_2)}(\mathbf{p})$ are

$$\begin{aligned}\varphi_n^{\max}(p) &= \xi_2[\pi n - (\tau E_b + 2\phi_{12})/2 - \tau p^2/4]/2, \\ \varphi_n^{\mathrm{zero}}(p) &= \xi_2[\pi/2 + \pi n - (\tau E_b + 2\phi_{12})/2 - \tau p^2/4]/2. \end{aligned} \tag{32}$$

Equations (32) define Fermat (or Archimedean) spirals (or helixes) in the (p,φ) plane. As $\varphi_n^{\max}(p)$ and $\varphi_n^{\mathrm{zero}}(p)$, shifted by the angle $\pi/4$ with respect to each other, vary with energy $p^2/2$ (through possibly many 2π cycles, depending upon τ), they trace out the maxima and the zeros of the TDP $\mathcal{W}_{\xi_2}^{\xi_1(\Gamma_1,\Gamma_2)}$. Since $|\xi_2| = 1$, the pattern is a *four-arm* helical spiral, corresponding to $n = 0,1,2,3$, as other values of n replicate the same lines. However, depending on the relative strength of interferences between the pathways Γ_{12} and the pathways Γ_1 and Γ_2 [see the last term in the TDP (28)], the *four*-start vortices may be modified by such interferences.

Our numerical results for these PT predictions for two oppositely circularly polarized six-cycle pulses are shown in Fig. 4, where we plot the ionized-electron momentum distributions in the polarization plane ($\theta = \pi/2$) for an intensity of 1 TW/cm^2 and various CEPs and time delays. Regardless of the time delay between the two pulses, the four spots or arms seen in Figs. 4(a)–4(f) indicate that the leading term in the ionized electron momentum distributions stems from the amplitudes for the paths Γ_1 and Γ_2. The formula (31) for the TDP, which excludes the cross channel amplitudes, does capture the essential physics. Our numerical results for the formula (31) (in which only $L = 2, M_L = \pm 2$ amplitudes are included) are shown in Fig. 5. In Eq. (31) the assumed equal dynamical parameters $\mathcal{M}_d^{(1)}(p) \simeq \mathcal{M}_d^{(2)}(p) \equiv \mathcal{M}_d(p)$ are extracted numerically from an *ab initio* TDSE calculation for a *single* pulse (as described in Appendix B). Thus, comparing Figs. 4 and 5 probes qualitatively the contribution of the pathways Γ_{12} relative to the direct pathways Γ_1 and Γ_2.

Results shown in Figs. 4(a) and 4(b) or in Figs. 5(a) and 5(b) are for zero time delay between the two pulses and two values of the relative CEP ϕ_{12}. For $\tau = 0$, superposing two oppositely circularly polarized pulses gives a linearly polarized pulse. We observe in Fig. 5(a) the expected symmetric quadrupole pattern [$\propto \cos^2(2\xi_1\varphi)$, see Eq. (31)] of the ionized electron momenta along both the linear polarization axis, which for $\phi_{12} = 0$ is the p_x axis ($\varphi = 0,\pi$), and the perpendicular p_y axis ($\varphi = -\pi/2,\pi/2$). A similar result is shown in Fig. 5(b) except that here $\phi_{12} = -\pi/2$ so that the linear polarization axis is rotated clockwise by $\varphi = \pi/4$, giving an angular distribution $\propto \cos^2(\phi_{12}/2 - 2\xi_1\varphi)$ from Eq. (31). For $\phi_{12} \neq 0$, a change in sign of ξ_1 will change the angular distribution, unlike when $\phi_{12} = 0$. This sensitivity to the helicity of ξ_1 is essential for producing vortices when the time delay is nonzero.

For zero time delay and any relative phase ϕ_{12} the four peaks in the quadrupole patterns have the same intensity in Figs. 5(a) and 5(b), as expected by formula (31). However, in Figs. 4(a) and 4(b), whereas the two spots along the linear polarization axis have the same brightness, those along its perpendicular axis are less bright. This difference in the brightness of the quadrupole pattern is due to the interferences between the paths Γ_{12} with the paths Γ_1 and Γ_2, as the last term in the TDP (28) for $\varphi = 0,\pi$ and that for $\varphi = -\pi/2,\pi/2$ have opposite signs.

For nonzero time delay between the two pulses, we obtain the vortex patterns shown in Figs. 4(c)–4(f) and Figs. 5(c)–5(f) for right and left circularly polarized pulses. As discussed above, these are *four*-start Fermat spiral patterns with a counterclockwise handedness. As predicted by Eqs. (32), the number and locations of the maxima and minima of the TDP in the polarization plane depend on the time delay, as shown in Figs. 4(c)–4(f) and Figs. 5(c)–5(f). For our pair of pulses, each having six optical cycles, the pulse duration is about 1.65 fs. Figures 4(c)–4(f) show that several hundred attoseconds are necessary to observe well-defined vortex patterns. The matter-wave vortex patterns in the electron momentum distributions shown in Figs. 4(c)–4(f) for four time delays are similar to

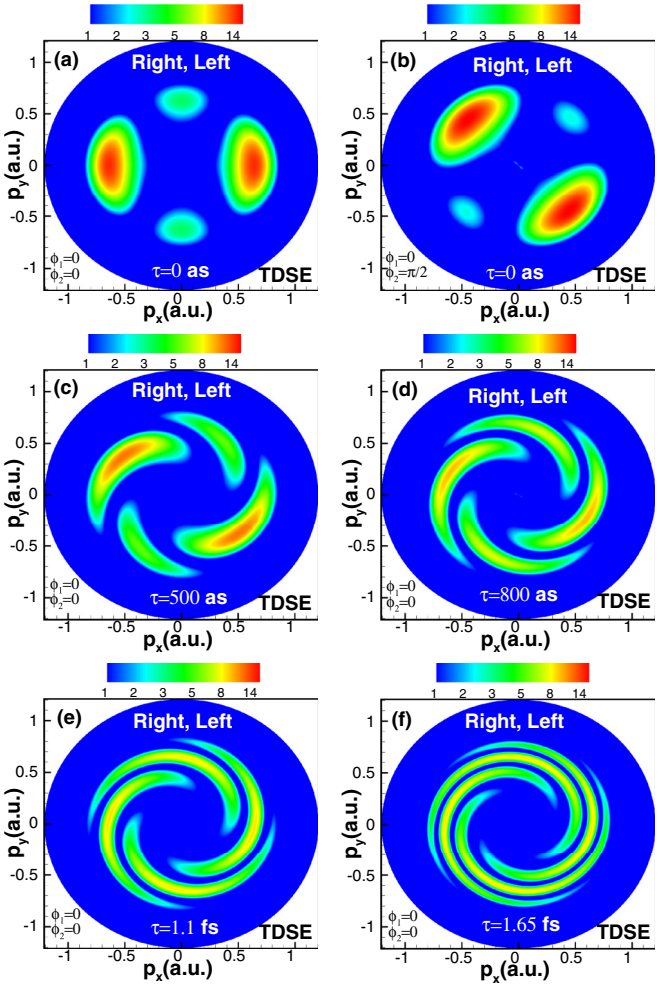

FIG. 4. *Four*-start spiral vortex patterns in the photoelectron momentum distributions $d^3W/d^3\mathbf{p}$ [see Eq. (5)] in the polarization plane following ionization of helium by right and left circularly polarized pulses delayed in time by (a) and (b) $\tau = 0$, (c) $\tau = 500$ as, (d) $\tau = 800$ as, (e) $\tau = 1.1$ fs, and (f) $\tau = 1.65$ fs. In (a) and (c)–(f), $\phi_1 = \phi_2 = 0$; in (b), $\phi_1 = 0$, $\phi_2 = \pi/2$. Each pulse has $\omega_1 = 15$ eV, $N = 6$ cycles, and $I = 10^{12}$ W/cm^2. The magnitudes of the TDPs (in units of 10^{-7} a.u.) are indicated by the color scales. In all panels, the numerical projections (5) include $L = 0,2$ with $M_L = 0,\pm 2$.

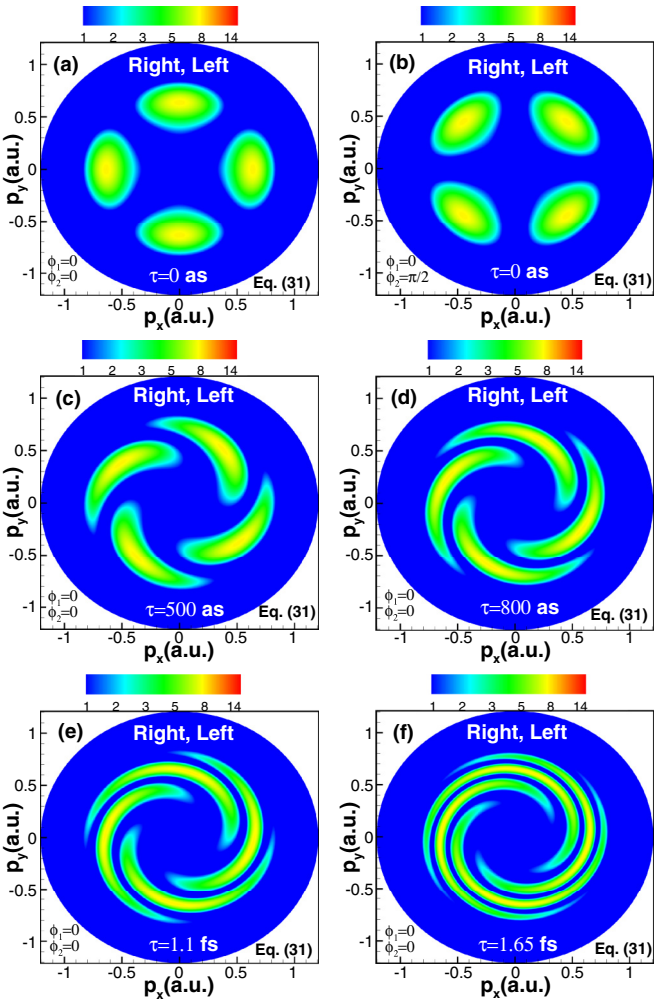

FIG. 5. Same as Fig. 4 but the numerical results are obtained using the PT formulas (31) and (20) with the dynamical parameter $\mathcal{M}_d(p)$ extracted numerically from *ab initio* TDSE calculations for a *single* pulse including *only* $L = 2, M_L = \pm 2$ amplitudes (see Appendix B). Note that Eq. (31) excludes cross channel contributions.

the interference fringes of optical beams of opposite helicities carrying orbital angular momentum of two [9]. In both cases the interference patterns are *four*-start Fermat spirals whose orientation is determined by the relative phase difference. In our case, this phase difference Φ is determined by the energy $(p^2/2 + E_b)$, the time delay τ, and ϕ_{12}, while in the optical case the relative phase is determined by the wave-front curvature difference [9]. In neither case is the appearance of helical fringes caused by the polarization of either the optical or electronic waves. Indeed, in the optical case both light beams were linearly polarized [9], and in our electronic case, the electron states with $L_z = \pm 2$ are dominant and populated equally upon ionization by the pair of oppositely circularly polarized pulses.

Note that for nonzero time delays τ shorter than about 800 as, the above-mentioned difference in the brightness in the quadrupole pattern persists [see Figs. 4(c) and 4(d) and Figs. 5(c) and 5(d)], which is a signature of the cross channels Γ_{12}. However, for time delays τ greater than 1.1 fs, both the *ab initio* TDSE results in Figs. 4(e) and 4(f) and the PT results in Figs. 5(e) and 5(f) are in very good agreement.

To better understand the sensitivity of the τ-dependent ionization cross channels to the handedness of the two pulses, we present in Figs. 6 and 7 respectively the ionized-electron energy and angular distributions in the polarization plane for four values of the time delay. In Fig. 6 the ionized electrons are detected at the angles $\theta = \pi/2, \varphi = 0$, whereas in Fig. 7 the final electron kinetic energy is $E = 2\omega_1 - E_b$. Plotted in these two figures are (i) TDSE results for final states $L = 0,2; M_L = 0,\pm 2$, (ii) TDSE results for final states $L = 2; M_L = \pm 2$, and (iii) numerical results using formula (31) for final states $L = 2; M_L = \pm 2$. For shorter time delays $0 \leqslant \tau < 1.1$ fs [see Figs. 7(a)–7(c)], the angular distributions obtained from the results (ii) and (iii) exhibit a fourfold symmetric quadrupolelike shape, while those from the results (i) exhibit a twofold symmetric quadrupolelike shape. All these

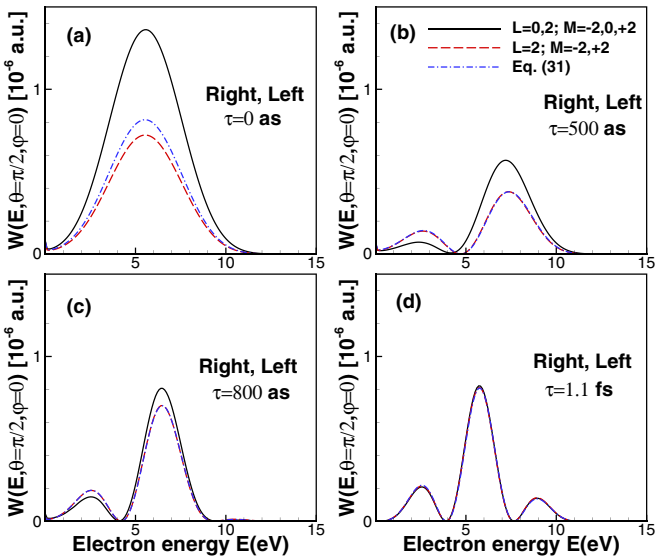

FIG. 6. Energy distributions in the polarization plane for electrons detected at the angle $\varphi = 0$ following two-photon single ionization of He by two oppositely circularly polarized pulses delayed in time by (a) $\tau = 0$ as, (b) $\tau = 500$ as, (c) $\tau = 800$ as, and (d) $\tau = 1.1$ fs. Parameters of the two pulses are the same as in Fig. 4. Results are obtained from TDSE calculations for the following final states: (i) $L = 0,2$ with $M_L = 0,\pm 2$ (solid black lines), (ii) $L = 2$ with $M_L = \pm 2$ (dashed red lines); and from the formula (31), in which the dynamical parameter $\mathcal{M}_d(p)$ is extracted numerically (as described in Appendix B) from an *ab initio* TDSE calculation for a single pulse including only $L = 2, M_L = \pm 2$ amplitudes (dash-dotted blue lines).

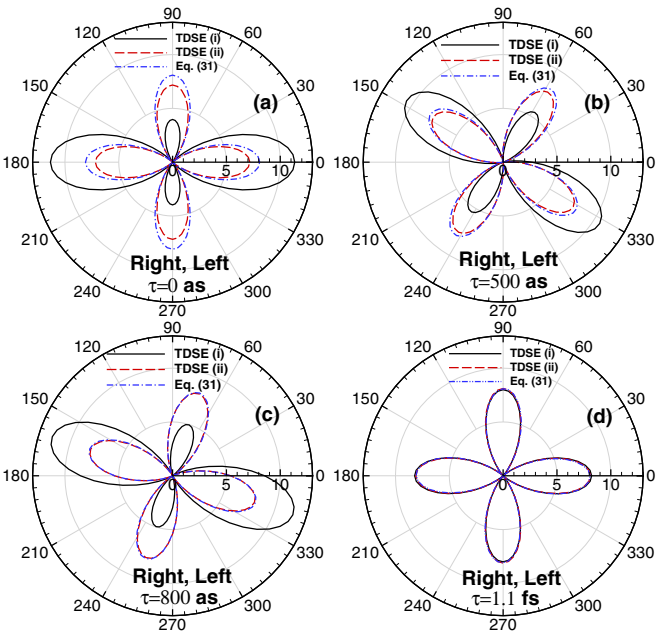

FIG. 7. Angular distributions $d^3W/d^3\mathbf{p}$ (in units of 10^{-7} a.u.) in the polarization plane for a fixed ionized electron energy of $E = 2\omega_1 - E_b$ following two-photon single ionization of He by two oppositely circularly polarized pulses delayed in time by (a) $\tau = 0$ as, (b) $\tau = 500$ as, (c) $\tau = 800$ as, and (d) $\tau = 1.1$ fs. Parameters of the two pulses are the same as in Fig. 4. Results are obtained from TDSE calculations for the following final states: (i) $L = 0,2$ with $M_L = 0,\pm 2$ (solid black lines), (ii) $L = 2$ with $M_L = \pm 2$ (dashed red lines); and from the formula (31) as described in the caption of Fig. 6 (dash-dotted blue lines).

angular distribution shapes are consistent with those of the spherical harmonic $Y_{L,M_L}(\hat{\mathbf{p}})$. Both Figs. 6 and 7 show that the TDSE results (ii) and the results using Eq. (31) are in good agreement regardless of the time delay. Moreover, whereas these two results and the TDSE results (i) differ significantly for zero time delay and for time delays shorter than 1.1 fs [see Figs. 6(a)–6(c) and Figs. 7(a)–7(c)] owing to the role played by the path Γ_{12}, they coincide for a time delay equal to $\tau_c = 1.1$ fs [see Figs. 6(d) and 7(d)] or longer (not shown). Since the τ_c found for two identical circularly polarized six-cycle pulses is also 1.1 fs, one can conclude that this critical time delay τ_c is at most only weakly sensitive to the handedness of the two circularly polarized pulses. Remarkably, for time delays longer than τ_c, the formula (31) (in which the ionization cross channels are omitted) becomes fully valid for reproducing the rather challenging six-dimensional TDSE results.

A substantial consequence of the validity of the formula (31) is that the time-delay periodicity of the angular distributions in the polarization plane is valid *only* for longer time delays (i.e., for $\tau \geqslant \tau_c$). Figure 8 shows the time-delay periodicity of the ionized-electron angular distributions in the polarization plane produced by our pair of oppositely circularly polarized six-cycle pulses for time delays longer than $\tau_c = 1.1$ fs. Results of our numerical solutions of the TDSE in Fig. 8(a) are compared with the results using Eq. (31) in Fig. 8(b) for a *fixed* electron kinetic energy, $E = 2\omega_1 - E_b$. For fixed relative CEP ϕ_{12} between the two pulses, the angular distribution is unchanged for time delays of $\tau_n = 2n\pi/(E + E_b)$ with n an integer, as expected from the PT Eqs. (31) and (20). Figure 8(b) shows that Eq. (31) is valid: the angular distributions for $\tau_8 = 1.1$ fs and $\tau_{12} = 1.65$ fs are identical. Our numerical results in Fig. 8(a) for these two time delays are exactly the same, indicating that for longer τ and for intensities $\sim$1 TW/cm^2 the second pulse sees the same initial state as the first pulse (i.e., the He ground state instead of the state resulting from interaction of the He ground state with the first attosecond pulse). For longer time delays τ_n with half odd integer n, the PT Eqs. (31) and (20) predict the angular distributions to be shifted by $\pi/4$ with respect to those for integer n, as shown in Figs. 8(a) and 8(b). This sensitivity of the angular distributions to the time delay implies the ability to control the ionized electron direction by adjusting the time delay between the two UV pulses.

For $\tau < \tau_c$, the ionization cross channels Γ_{12} (in which one photon is absorbed from each pulse) destroy the time-delay periodicity of the angular distributions (28) for two oppositely circularly polarized pulses. However, the parametrization (19) allows one to predict cases for which the τ periodicity of the TDP should be preserved even for $\tau < \tau_c$. Namely, let us consider the situation when one photon, say $\mathbf{e}_2$, is linearly polarized (i.e., $\ell_2 = 1$) in a direction perpendicular to the polarization plane of the first photon $\mathbf{e}_1$. In such cases, $\mathbf{e}_1 \cdot \mathbf{e}_2 = 0$. Further, suppose that the electrons are detected in the polarization plane of the first photon, so that one has $\hat{\mathbf{p}} \cdot \mathbf{e}_2 = 0$. Consequently, Eq. (19) for the amplitude $A^{\xi_1}_{\xi_2}(\mathbf{p})$

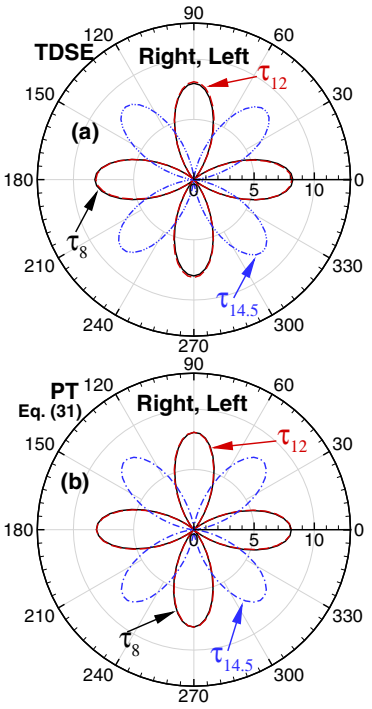

FIG. 8. Time-delay periodicity of electron angular distributions $d^3W/d^3\mathbf{p}$ (in units of 10^{-7} a.u.) in the polarization plane produced by two-photon single ionization of the He ground state by two oppositely circularly polarized UV pulses. The ionized-electron energy is fixed to be $E = 2\omega_1 - E_b$. Parameters of the two pulses are the same as in Fig. 4. Results in panel (a) are obtained by *ab initio* TDSE calculations for $L = 0,2$ with $M_L = 0,\pm 2$ final states; results in panel (b) are obtained using PT formula (31) calculated as described in the caption of Fig. 6. In each panel, results are shown for three time delays: τ_8, τ_{12}, and $\tau_{14.5}$, where $\tau_n = n\pi/\omega_1$.

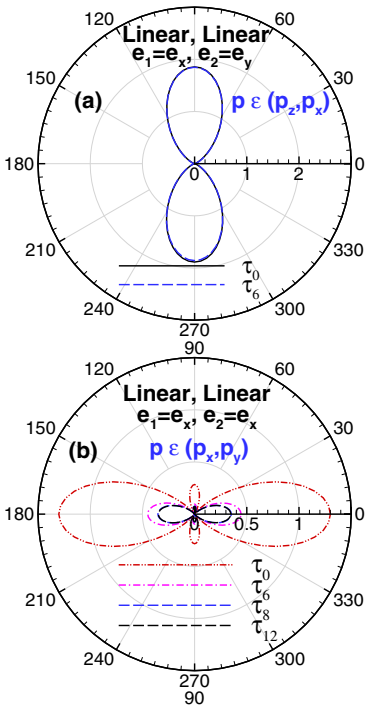

FIG. 9. Cross channel path (Γ_{12}) effects for two time-delayed linearly polarized pulses. (a) Angular distributions $d^3W/d^3\mathbf{p}$ (in units of 10^{-3} a.u.) in the (p_z, p_x) plane for two-photon single ionization of the He ground state by two time-delayed orthogonal pulses linearly polarized along the x and y axes, respectively. Results for time delays τ_0 and τ_6 are shown, where $\tau_n = n\pi/\omega_1$. (b) Angular distributions $d^3W/d^3\mathbf{p}$ (in units of 10^{-2} a.u.) in the (p_x, p_y) plane for two-photon single ionization of the He ground state by two time-delayed pulses linearly polarized along the x axis. Results for four time delays are shown, namely, τ_0, τ_6, τ_8, and τ_{12}. In both (a) and (b), the ionized electron energy is $E = 2\omega_1 - E_b$; each $\cos^2$ pulse has a carrier frequency $\omega_1 = 15$ eV, $N = 6$ cycles, an intensity of $I = 5 \times 10^{13}$ W/cm^2, and a zero CEP.

becomes

$$A^{\xi_1}_{\xi_2}(\mathbf{p}) = e^{-2i\phi_1}[\mathcal{M}_d(\hat{\mathbf{p}}\cdot\mathbf{e}_1)^2 + \mathcal{M}_{ds}(\ell_1 + e^{i\Phi})]. \quad (33)$$

The time delay τ enters this equation only through the phase Φ [see Eq. (20)], which means that the corresponding TDP should be periodic in τ as long as PT is valid. To demonstrate numerically this PT prediction for any time delay, we consider the case of two time-delayed orthogonal pulses that are linearly polarized along the x and y axes, respectively. Figure 9(a) shows the numerically calculated angular distributions for electrons detected in the (p_z, p_x) plane. One sees that results for the time delays $\tau = 0$ and $\tau_6 = T/2 = 827$ as (where $\tau_6 < \tau_c$) do coincide. The same observation holds for any time delays $\tau_n = n\pi/\omega_1$, where n is an integer.

Concerning the sensitivity to the pulse ellipticity of the ionization cross channels, we note that the formula (18) predicts a decreasing contribution of the cross channels as the time delay τ increases *not only* for circularly polarized pulses, but also for any two ellipticities of the two pulses. A numerical confirmation of this PT prediction is shown in Fig. 9(b) for the case of two pulses linearly polarized along the x axis with electrons detected in the (p_x, p_y) plane. Results shown are for four time delays: τ_0, $\tau_6 = T/2$, $\tau_8 = 2T/3$, and $\tau_{12} = T$, where $\tau_n = n\pi/\omega_1$. Once again, one sees in Fig. 9(b) that the TDP is maximal for $\tau = 0$ and then decreases as τ increases (as shown by the results for $\tau_6 = 827$ as and $\tau_8 = \tau_c = 1.1$ fs). However, the angular distributions for τ_8 and τ_{12} coincide, which confirms the time-delay periodicity prescribed by PT for $\tau \geqslant \tau_c$.

So far, the contributions of the ionization cross channels Γ_{12}, which are difficult to calculate, have been investigated by comparing results obtained by solving the TDSE to those obtained from PT formulas that include contributions from only the pathways Γ_1 and Γ_2. The question thus arises whether relevant information on the dynamical parameters describing the cross channels can be obtained by other means. First, we note that in contrast to corotating fields, a virtue of counter-rotating circularly polarized fields is that electric dipole selection rules naturally separate the three ionization pathways. Thus, counter-rotating circularly polarized fields seems to be the most suitable scheme for extracting the dynamical parameters $\Gamma^{(12)}(p,\theta,\tau)$ describing the cross channel contributions to the TDP. Second, although calculating the dynamical parameters $\mathcal{M}_d^{(12)}(p,\tau)$ and $\mathcal{M}_{ds}^{(12)}(p,\tau)$ on which $\Gamma^{(12)}(p,\tau)$ depends [see Eq. (29)] is not an easy task, by choosing a special detection geometry one can isolate the effect

of the dynamical parameters $\mathcal{M}_{ds}^{(12)}(p,\tau)$, which correspond to transitions to final states $L = 0,2$ with $M_L = 0$. This can be done by using counter-rotating fields and by detecting electrons along the pulse propagation direction (i.e., $\theta = 0$). In this case, $\hat{\mathbf{p}} \cdot \mathbf{e}_1 = \hat{\mathbf{p}} \cdot \mathbf{e}_2 = 0$, so that the TDP in Eq. (26) only depends upon $\mathcal{M}_{ds}^{(12)}(p,\tau)$.

V. SINGLE IONIZATION BY TWO-COLOR CIRCULARLY POLARIZED PULSES

In this section we consider the $(\omega_2 + 2\omega_1)$ process, i.e., the process of single ionization of He by interfering one-photon and two-photon ionization amplitudes in which the He atom can either absorb one ω_2 photon from the first pulse or two ω_1 photons from the second pulse [cf. Fig. 1(b)]. By focusing on the near-threshold ionized-electron energy range, $0 \leqslant E \leqslant 15$ eV, we only consider the ionization pathways Γ_1 and Γ_2 [Fig. 1(b)]. We thus neglect the contributions of the Γ_{12} pathways [not shown in Fig. 1(b)], which produce ionized electrons in the continuum with higher kinetic energies.

Within the dipole approximation [37], the PT amplitude $A_{\xi_2}^{\xi_1}(\mathbf{p})$ for one-photon or two-photon ionization by a pair of arbitrarily polarized pulses is

$$A_{\xi_2}^{\xi_1}(\mathbf{p}) = e^{-i\phi_1}[\alpha(p)(\mathbf{e}_1 \cdot \hat{\mathbf{p}}) + \mathcal{M}_d(p)(\mathbf{e}_2 \cdot \hat{\mathbf{p}})^2 e^{i\tilde{\Phi}}], \quad (34)$$

where $\tilde{\Phi} \equiv \Phi - \phi_1$, with the relative phase Φ given by Eq. (20), and the p-dependent dynamical parameter $\alpha(p)$ [8] is the product of the dipole moment of the target and $\hat{F}_0(E + E_b - \omega_2)$, the Fourier transform of the pulse envelope [cf. Eq. (11)]. According to electric dipole selection rules, the dynamical parameter $\alpha(p)$ corresponding to the path Γ_1 describes a one-photon absorption transition from the initial S state to final P states. Likewise, the p-dependent dynamical parameter $\mathcal{M}_d(p)$ [cf. Eq. (9)] corresponding to the path Γ_2 describes a two-photon absorption transition to final D states. Since the final states reached by these two interfering pathways have opposite parities, the photoelectron angular distributions are expected to be asymmetric.

For two circularly polarized pulses with the same handedness, $\mathbf{e}_1 = \mathbf{e}_2 = \mathbf{e}$, $\ell_1 = \ell_2 = \ell = 0$, and $\xi_1 = \xi_2 = \xi = \pm 1$, so that the PT amplitude (34) takes the form

$$A_{\xi}^{\xi}(\mathbf{p}) = e^{-i\phi_1}(\mathbf{e} \cdot \hat{\mathbf{p}})[\alpha(p) + \mathcal{M}_d(\mathbf{e} \cdot \hat{\mathbf{p}}) e^{i(\Phi - \phi_1)}], \quad (35)$$

where the geometric factor $(\mathbf{e} \cdot \hat{\mathbf{p}})$ is

$$(\mathbf{e} \cdot \hat{\mathbf{p}}) = (1/\sqrt{2}) \sin\theta e^{\pm i\varphi} \propto Y_{1,M_1}(\theta,\varphi). \quad (36)$$

According to the geometric factors (36) and (22), such a pair of pulses produces final states defined by $L = 1,2$, with $M_1 = +1, M_2 = +2$ ($M_1 = -1, M_2 = -2$) for two right (left) circularly polarized pulses.

Likewise, for two oppositely circularly polarized two-color pulses, $\mathbf{e}_1 = \mathbf{e}_2^*$, $\ell_1 = \ell_2 = 0$, and $\xi_1 = -\xi_2 = \pm 1$. Thus, the PT amplitude (34) in this case takes the form

$$A_{\xi_2}^{\xi_1}(\mathbf{p}) = e^{-i\phi_1}[\alpha(p)(\mathbf{e}_1 \cdot \hat{\mathbf{p}}) + \mathcal{M}_d(p)(\mathbf{e}_1^* \cdot \hat{\mathbf{p}})^2 e^{i\tilde{\Phi}}], \quad (37)$$

where the final states defined by $L = 1,2$, with $M_1 = +1, M_2 = -2$ ($M_1 = -1, M_2 = +2$) are produced by right and left (left and right) circularly polarized pulses.

Substituting the geometric factors (22) and (36) into the PT amplitudes in Eqs. (35) and (37), the TDP (6) for single ionization by our two-color pulses circularly polarized in the same or opposite directions is

$$\mathcal{W}_{\xi_2}^{\xi_1}(p,\theta,\varphi) = \frac{\mathcal{C}}{2}\sin^2\theta\Big\{|\alpha(p)|^2 + \frac{1}{2}\sin^2\theta|\mathcal{M}_d(p)|^2 + \sqrt{2}\sin\theta|K_{12}| \times \big(2\cos^2[(\Phi - \phi_1 + \Theta_{12} + \xi_{12}\varphi)/2] - 1\big)\Big\}, \quad (38)$$

where Φ is defined in Eq. (20), $\xi_{12} = +1(-1)$ for two right (left) circularly polarized pulses, and $\xi_{12} = -3(+3)$ for right and left (left and right) circularly polarized pulses; the modulus of the dynamical parameter $K_{12}(p) \equiv |K_{12}(p)|e^{i\Theta_{12}(p)}$ is

$$|K_{12}(p)| = \sqrt{\{\mathrm{Re}\,[\alpha^*(p)\mathcal{M}_d(p)]\}^2 + \{\mathrm{Im}\,[\alpha^*(p)\mathcal{M}_d(p)]\}^2}, \quad (39)$$

and its argument is defined by

$$\tan\Theta_{12}(p) = \frac{\mathrm{Im}\,[\alpha^*(p)\mathcal{M}_d(p)]}{\mathrm{Re}\,[\alpha^*(p)\mathcal{M}_d(p)]}. \quad (40)$$

The ionized-electron angular distribution (38) in the polarization plane ($\theta = \pi/2$) has the form of a *one-start* or *three-start* spiral structure depending upon the handedness of each of the two pulses, as may be seen from the following considerations. From Eq. (38), the TDP $\mathcal{W}_{\xi_2}^{\xi_1}$ is maximal for $(\Phi - \phi_1 + \Theta_{12})/2 + \xi_{12}\varphi/2 = \pi n$ and is minimal for $(\Phi - \phi_1 + \Theta_{12})/2 + \xi_{12}\varphi/2 = (2n+1)\pi/2$, where $n = 0, \pm 1, \pm 2 \ldots$, and $0 \leqslant \varphi \leqslant 2\pi$. Using Eq. (20), the p dependencies of the polar angles φ at these maximum and minimum values of $\mathcal{W}_{\xi_2}^{\xi_1}(p,\theta,\varphi)$ are

$$\begin{aligned}\varphi_n^{\max}(p) &= [2\pi n - (\tau E_b + \tilde{\Theta}_{12}) - \tau p^2/2]/\xi_{12},\\ \varphi_n^{\min}(p) &= [\pi + 2\pi n - (\tau E_b + \tilde{\Theta}_{12}) - \tau p^2/2]/\xi_{12},\end{aligned} \quad (41)$$

where $\tilde{\Theta}_{12}(p,\phi_1,\phi_2)$ is given by

$$\tilde{\Theta}_{12}(p,\phi_1,\phi_2) = \phi_1 - 2\phi_2 + \Theta_{12}(p). \quad (42)$$

Equations (41) define Fermat (or Archimedean) spirals (or helixes) in the (p,φ) plane, which are modified by the CEP and p dependencies of the phase $\tilde{\Theta}_{12}(p,\phi_1,\phi_2)$. As $\varphi_n^{\max}(p)$ and $\varphi_n^{\min}(p)$, shifted by the angle π or $\pi/3$ with respect to each other, vary with energy $p^2/2$ (through possibly many 2π cycles, depending upon τ), they trace out the maxima and the minima of the TDP. When $|\xi_{12}| = 1$ ($|\xi_{12}| = 3$), the pattern is a *one-arm* (*three-arm*) helical spiral, corresponding to $n = 0$ ($n = 0,1,2$), as other values of n replicate the same lines. Pulses with $\xi_{12} = \pm 1$ ($\xi_{12} = \pm 3$) correspond to counterclockwise (+) or clockwise (−) spirals. The Fermat spirals become wound more densely as τ increases.

For our calculations of the *odd*-start electron vortices, we consider that the first (second) six-cycle pulse has a carrier frequency $\omega_2 = 30$ eV ($\omega_1 = 15$ eV), an intensity $I_2 = 10^{13}$ W/cm^2 ($I_1 = 10^{14}$ W/cm^2), and a total duration of 827 as (1.65 fs). The intensity of each pulse is chosen such

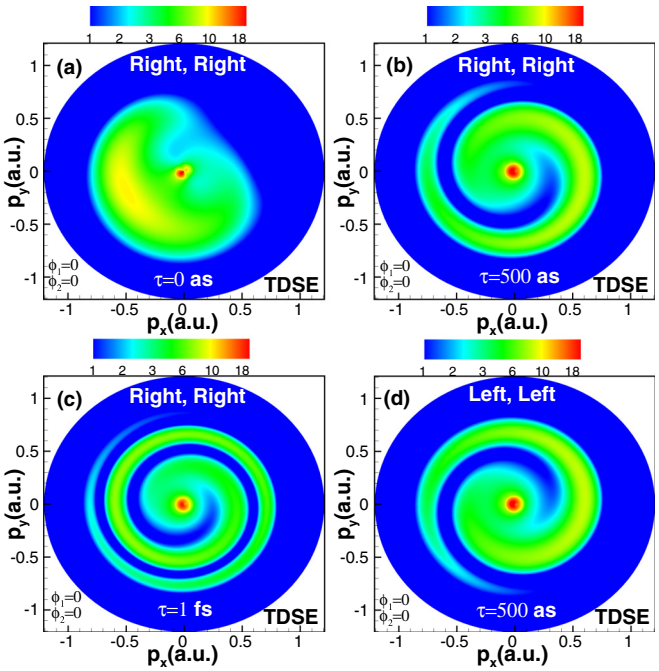

FIG. 10. One-start spiral vortex patterns in the electron momentum distribution $d^3W/d^3\mathbf{p}$ [see Eq. (5)] in the polarization plane following one-photon or two-photon single ionization of He by two identical circularly polarized pulses for three time delays: (a) $\tau = 0$, (b),(d) $\tau = 500$ as, and (c) $\tau = 1$ fs. In (a)–(c), the two pulses are both right circularly polarized, whereas in (d) they are both left circularly polarized. The carrier frequency and intensity of the earlier (later) pulse is $\omega_2 = 30$ eV ($\omega_1 = 15$ eV) and $I_2 = 10$ TW cm^{-2} ($I_1 = 100$ TW cm^{-2}). The magnitudes of the TDPs (in units of 10^{-3} a.u.) are indicated by the color scales.

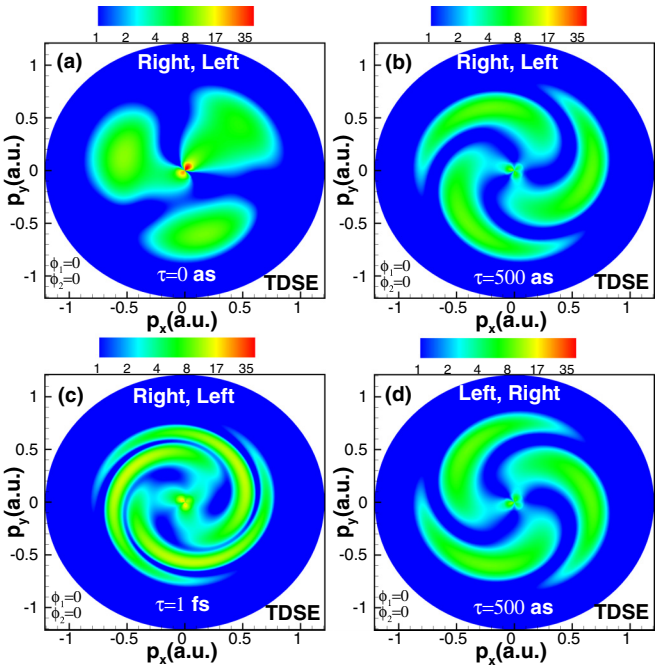

FIG. 11. Three-start spiral vortex patterns in the electron momentum distribution $d^3W/d^3\mathbf{p}$ [see Eq. (5)] in the polarization plane following one-photon or two-photon single ionization of He by two oppositely circularly polarized pulses for three time delays: (a) $\tau = 0$, (b),(d) $\tau = 500$ as, and (c) $\tau = 1$ fs. In (a)–(c), pulses are right and left circularly polarized, whereas in (d) they are left and right circularly polarized. The pulse parameters are the same as in Fig. 10. The magnitudes of the TDPs (in units of 10^{-3} a.u.) are indicated by the color scales.

that one-photon absorption from the first pulse and two-photon absorption from the second pulse photoionize the He atom with comparable magnitudes and produce photoelectrons with the same kinetic energy.

For our two-color circularly polarized pulses having the same or opposite handedness and zero CEPs, our numerical results for these PT predictions of *one*-start and *three*-start electron vortices [cf. Eqs. (38) and (41)] are shown in Figs. 10 and 11, respectively, for several time delays. We consider first the case of zero time delay. For co-rotating pulses, the calculated momentum distribution in the polarization plane ($\theta = \pi/2$) is shown in Fig. 10(a). The TDP exhibits a broad single crescent-shaped lobe along the p_x axis but shifted counterclockwise by a certain angle. For counter-rotating pulses, the corresponding momentum distribution is shown in Fig. 11(a). The TDP exhibits three lobes separated by $2\pi/3$. These two findings are consistent with our PT formula (38) as the TDP is $\propto \cos^2\{[\Theta_{12}(p) + \xi_{12}\varphi]/2\}$, in which $\xi_{12} = +1$ for two right circularly polarized pulses and $\xi_{12} = -3$ for right and left circularly polarized pulses. A change in sign of ξ_{12} will change the angular distribution, unlike when $\phi_{12} = 0$ for the case of single-color two-photon interferometry. This unusual sensitivity to the helicity of ξ_{12}, which leads to a circular dichroic effect, is caused by the dynamical phase $\Theta_{12}(p)$ [cf. Eq. (40)] involving interference between the one-photon path Γ_1 and the two-photon path Γ_2. To reproduce numerically these TDSE results, using the PT Eq. (38), requires an accurate calculation of both the phase and the modulus of the dynamical parameter $K_{12}(p)$, which includes pulse overlap effects.

For nonzero time delay between the two corotating pulses, one obtains the vortex patterns in the ionized electron momentum distributions shown in Figs. 10(b) and 10(c) for two-color right circularly polarized pulses, and in Fig. 10(d) for two-color left circularly polarized pulses. For counter-rotating pulses, we obtain the vortex patterns shown in Figs. 11(b) and 11(c) for two-color right and left circularly polarized pulses, and in Fig. 11(d) for two-color left and right circularly polarized pulses. As discussed above, for corotating pulses these are *one*-start Fermat spiral patterns with opposite handedness, i.e., clockwise in Figs. 10(b) and 10(c) and counterclockwise in Fig. 10(d). Likewise, for counter-rotating pulses, these are *three*-start Fermat spiral patterns with opposite handedness, i.e., counterclockwise in Figs. 11(b) and 11(c) and clockwise in Fig. 11(d). As predicted by the helix equation (41), for both corotating and counter-rotating pulses the numbers and locations of the maxima and minima of the TDP in the polarization plane depend on the time delay, as shown in Figs. 10(b)–10(d) and 11(b)–11(d). For our two-color (ω and 2ω) pulses with durations of 827 as and 1.65 fs, we show that time delays of several hundred attoseconds are necessary to produce a complete revolution of the *odd*-start spirals.

VI. SUMMARY AND CONCLUSIONS

By both an analytic PT analysis and numerical solutions of the six-dimensional TDSE for single ionization of the He atom by a pair of time-delayed circularly polarized ultrashort laser pulses, we have investigated the conditions under which the photoelectron momentum distributions in the laser pulse polarization plane have the form of *multistart* electron vortices. For single-color two-photon interferometry, we have shown that the ionized-electron momentum distributions in the polarization plane exhibit *zero*-start or *four*-start spiral vortex patterns for the cases respectively of corotating or counter-rotating pulses. Regardless of the ellipticity or handedness of the two pulses, the contributions of the ionization cross channels Γ_{12} were found to decrease as the time delay τ increases, in agreement with PT. For short time delays τ such that there is strong overlap between the two pulses, these cross channels were found to be as important as the leading ionization channels, Γ_1 and Γ_2. However, for longer time delays the cross channel contributions are very small and, consequently, Eq. (31) (in which their contributions are excluded) becomes an excellent tool for describing accurately the ultrafast process of two-photon single ionization of helium. For the two-color process we investigated, we have shown that corotating or counter-rotating time-delayed fields produce *one*-start or *three*-start spiral vortex patterns in the photoelectron momentum distributions in the polarization plane. We emphasize that in this case even corotating time-delayed circularly polarized pulses lead to vortices in the ionized electron momentum distribution. For both fundamental ultrafast atomic processes considered in this paper, our analytic PT analysis provided an invaluable means of interpreting our numerical TDSE results.

Experimental observation of these *multiarm* spiral vortex patterns in the ionized-electron momentum distributions requires single-color and two-color circularly polarized pulses with *low intensity* but with full control of the relative CEP and the time delay between the two pulses. The production of chiral attosecond pulses is a very active field of research [38–41]. Existing velocity-map-imaging or reaction microscope techniques provide the means for measuring ionized-electron momentum distributions.

Note that the analysis presented in this paper can be applied also for other atoms in which the ionized electron is initially in an s state, including, e.g., the H atom. We have presented our results for the He atom because it is the simplest atom to investigate experimentally and because we are able to treat all electron correlation effects essentially exactly by solving the six-dimensional, two-electron TDSE. Our predictions should hold also for theoretical calculations employing a single active electron (SAE) approximation, although in that case agreement with experimental results will depend upon the strength of electron correlation effects for the particular atom chosen for study. More generally, as noted in the Introduction as well as in Ref. [8] (including its Supplemental Material), the vortices we predict stem from zeros in a kinematical factor of the TDP that is determined by the detection geometry. The form of this kinematical factor is invariant to any specific initial state of the active electron in a target atom (or molecule); it only depends on the binding energy. Hence, vortex patterns in the ionized electron momentum distributions should be observed quite generally for any initial angular momentum of the active electron. However, if the bandwidth of the laser pulses allows ionization from multiple atomic subshells, then the observation of the vortices will depend upon the relative magnitudes of the subshell cross sections (as the vortex pattern for one subshell may be obscured by the momentum distributions of the other subshells).

Note added in proof. Very recently K.-J. Yuan *et al.* [45] demonstrated spiral vortex patterns in the electron momentum distributions resulting from ionization of the H_2^+ molecule by time-delayed bichromatic circularly polarized fields. As noted in Secs. I and VI above, the spiral vortex patterns in the ionized momentum distributions stem from kinematic factors, which are independent of the dynamical transition amplitudes that depend on the target species. Thus, as Ref. [45] nicely illustrates, these spiral vortex patterns appear also in molecular photoionization processes.

ACKNOWLEDGMENTS

Research of A.F.S. and J.M.N.D. was primarily supported by the U.S. Department of Energy (DOE), Office of Science, Basic Energy Sciences (BES), under Award No. DE-FG03-96ER14646; research of S.X.H. was supported by the DOE National Nuclear Security Administration under Award No. DE-NA0001944, the University of Rochester, and the New York State Energy Research and Development Authority; research of L.B.M. was supported by ERC-StG (Project No. 277767 - TDMET) and the VKR Center of Excellence, QUSCOPE; research of N.L.M. and A.V.M. was supported by the Ministry of Education and Science of the Russian Federation, under Project No. 1019. Computations were carried out using the Sandhills, Tusker, and Crane computing facilities of the Holland Computing Center at the University of Nebraska-Lincoln, as well as Stampede (TACC) under NSF Grant No. TG-PHY-120003.

APPENDIX A: DERIVATION OF THE SECOND-ORDER PT AMPLITUDE IN EQ. (7)

The second-order amplitude for single ionization of He by a pair of arbitrarily polarized pulses [see Fig. 1(a)] is given by [42]

$$A_2 = -\sum_{q\neq i}\int_{-\infty}^{\infty}\langle \nu\mathbf{p}|\mathbf{d}\cdot\mathbf{F}(t)|q\rangle\, e^{i\omega_{fq}t} \times \int_{-\infty}^{t}\langle q|\mathbf{d}\cdot\mathbf{F}(t')|i\rangle\, e^{i\omega_{qi}t'}\,dt'dt, \tag{A1}$$

where we have set the upper limit of the time variable to infinity since the pulse is short. In Eq. (A1) $|i\rangle$ is the two-electron initial state with energy E_i; $|\nu\mathbf{p}\rangle$ is the two-electron final state (satisfying incoming wave boundary conditions and comprising the bound state $|\nu\rangle$ of the residual ion, with energy E_ν, and the continuum state $|\mathbf{p}\rangle$ of the electron, with momentum $\mathbf{p}$ and energy $E = p^2/2$ [43,44]); $|q\rangle$ is a two-electron intermediate state with energy E_q; $\omega_{fq} \equiv E + E_\nu - E_q$; $\omega_{qi} \equiv E_q - E_i$; $\mathbf{d}$ is the electric dipole moment operator of the two electrons; and $\mathbf{F}(t)$ is the electric field (2), where $\omega^{(1,2)} \equiv \omega$ for the process

in Fig. 1(a). Equation (A1) involves integrals over time and space that are evaluated below.

The structure of the integrals over time in Eq. (A1) is

$$I = \int_{-\infty}^{\infty} [\mathbf{a}_1 \cdot \mathbf{F}(t)] e^{i\omega_{fq}t} \int_{-\infty}^{t} [\mathbf{a}_2 \cdot \mathbf{F}(t')] e^{i\omega_{qi}t'} dt' dt, \quad \text{(A2)}$$

where $\mathbf{a}_1 = \langle \nu\mathbf{p}|\mathbf{d}|q\rangle$, $\mathbf{a}_2 = \langle q|\mathbf{d}|i\rangle$. Inserting Eq. (2) into Eq. (A1) we obtain four integrals over time,

$$I = I_{11} + I_{12}(\tau) + I_{21}(\tau) + I_{22}(\tau), \quad \text{(A3)}$$

where the subscripts indicate the pulses that contribute to the two-photon transition (e.g., I_{11} indicates that both photons originate from the first pulse, while I_{12} indicates that one photon originates from the first pulse and the other originates from the second pulse, etc.). Let us consider first the integral I_{11}:

$$I_{11} = \int_{-\infty}^{\infty} F_0(t) \big(\mathbf{a}_1 \cdot \mathrm{Re}\,[\mathbf{e}_1 e^{-i(\omega t+\phi_1)}]\big) e^{i\omega_{fq}t} dt \times \int_{-\infty}^{t} F_0(t')(\mathbf{a}_2 \cdot \mathrm{Re}\,[\mathbf{e}_1 e^{-i(\omega t'+\phi_1)}]) e^{i\omega_{qi}t'} dt'. \quad \text{(A4)}$$

By extracting the vector dependence of Eq. (A4), one has

$$I_{11} = e^{-2i\phi_1} (\mathbf{a}_1 \cdot \mathbf{e}_1)(\mathbf{a}_2 \cdot \mathbf{e}_1)\, J_{11}^{++} + (\mathbf{a}_1 \cdot \mathbf{e}_1)(\mathbf{a}_2 \cdot \mathbf{e}_1^*) J_{11}^{+-} + (\mathbf{a}_1 \cdot \mathbf{e}_1^*)(\mathbf{a}_2 \cdot \mathbf{e}_1) J_{11}^{-+} + e^{2i\phi_1} (\mathbf{a}_1 \cdot \mathbf{e}_1^*)(\mathbf{a}_2 \cdot \mathbf{e}_1^*)\, J_{11}^{--}, \quad \text{(A5)}$$

where the parameters $J_{11}^{\pm\pm}$ describing two-photon absorption $(++)$ and two-photon emission $(--)$ are

$$J_{11}^{\pm\pm} = \frac{1}{4} \int_{-\infty}^{\infty} F_0(t)\, e^{i(\omega_{fq} \mp \omega)t} \int_{-\infty}^{t} F_0(t')\, e^{i(\omega_{qi} \mp \omega)t'} dt' dt, \quad \text{(A6)}$$

whereas the parameters $J_{11}^{\pm\mp}$ describing one-photon absorption or one-photon emission $(+-)$ and one-photon emission or one-photon absorption $(-+)$ are

$$J_{11}^{\pm\mp} = \frac{1}{4} \int_{-\infty}^{\infty} F_0(t)\, e^{i(\omega_{fq} \mp \omega)t} \int_{-\infty}^{t} F_0(t')\, e^{i(\omega_{qi} \pm \omega)t'} dt' dt. \quad \text{(A7)}$$

Based on our PT assumption (cf. Sec. III), the terms involving photon emission, i.e., J_{11}^{--} and $J_{11}^{\pm\mp}$, in Eq. (A5) are negligible. Thus, Eq. (A5) becomes

$$I_{11} = e^{-2i\phi_1} (\mathbf{a}_1 \cdot \mathbf{e}_1)(\mathbf{a}_2 \cdot \mathbf{e}_1)\, J_{11}^{++}. \quad \text{(A8)}$$

To evaluate the two-photon absorption term J_{11}^{++} [cf. Eq. (A6)] in Eq. (A8), we express the envelope function $F_0(t)$ as the inverse of its Fourier transform [Eq. (11)]:

$$F_0(t) = \frac{1}{2\pi} \int_{-\infty}^{\infty} \hat{F}_0(\epsilon)\, e^{-i\epsilon t} d\epsilon. \quad \text{(A9)}$$

Inserting this equation into Eq. (A6), the two time integrals reduce to a single integral over ϵ:

$$J_{11}^{++} = -\frac{i}{8\pi} \int_{-\infty}^{\infty} \frac{\hat{F}_0(\epsilon)\hat{F}_0(\omega_{fi} - 2\omega - \epsilon)}{E_q + \epsilon - (E_f - \omega) + i0} d\epsilon. \quad \text{(A10)}$$

One obtains similar analytical forms for $I_{12}(\tau)$, $I_{21}(\tau)$, and $I_{22}(\tau)$ by using the procedure employed [i.e., Eqs. (A4)–(A10)] for evaluating I_{11}. The time integral (A3) thus becomes

$$I = e^{-2i\phi_1} (\mathbf{a}_1 \cdot \mathbf{e}_1)(\mathbf{a}_2 \cdot \mathbf{e}_1) J_{11}^{++} + e^{-i\chi} (\mathbf{a}_1 \cdot \mathbf{e}_1)(\mathbf{a}_2 \cdot \mathbf{e}_2) \times J_{12}^{++}(\tau) + e^{-i\chi} (\mathbf{a}_1 \cdot \mathbf{e}_2)(\mathbf{a}_2 \cdot \mathbf{e}_1) J_{21}^{++}(\tau) + e^{-2i(\phi_2 - \omega\tau)} (\mathbf{a}_1 \cdot \mathbf{e}_2)(\mathbf{a}_2 \cdot \mathbf{e}_2) J_{22}^{++}(\tau), \quad \text{(A11)}$$

where $\chi = \phi_1 + \phi_2 - \omega\tau$. Note that

$$J_{22}^{++}(\tau) = e^{i(\omega_{fi} - 2\omega)\tau} J_{11}^{++}, \quad \text{(A12)}$$

i.e., the last term in Eq. (A11) describing two-photon absorption from the second pulse acquires an additional phase $e^{i\omega_{fi}\tau}$. The τ-dependent parameter J_{12}^{++} in Eq. (A11) describing one-photon absorption from the first pulse and one-photon absorption from the second pulse is

$$J_{12}^{++}(\tau) = -\frac{i}{8\pi} e^{i(\omega_{fi} - 2\omega)\tau} \times \int_{-\infty}^{\infty} \frac{\hat{F}_0(\epsilon)\, \hat{F}_0(\omega_{fi} - 2\omega - \epsilon)}{E_q + \epsilon - (E_f - \omega) + i0} e^{-i\epsilon\tau} d\epsilon, \quad \text{(A13)}$$

whereas the τ-dependent parameter J_{21}^{++} describing one-photon absorption from the second pulse and one-photon absorption from the first pulse is

$$J_{21}^{++}(\tau) = -\frac{i}{8\pi} \int_{-\infty}^{\infty} \frac{\hat{F}_0(\epsilon)\, \hat{F}_0(\omega_{fi} - 2\omega - \epsilon)}{E_q + \epsilon - (E_f - \omega) + i0} e^{i\epsilon\tau} d\epsilon. \quad \text{(A14)}$$

We focus now on the integration over angular variables of the second-order amplitude (A1). Within the PT approach, the first-order amplitude for one-photon absorption from a single pulse is defined by the matrix element

$$T^{(1)} = \langle \nu\mathbf{p}|\mathbf{e} \cdot \mathbf{d}|i\rangle, \quad \text{(A15)}$$

where $\mathbf{e}$ is the polarization vector of the pulse, $\mathbf{d}$ is the dipole moment of the two electrons, $|i\rangle$ is the initial $^1\mathrm{S}^e$ state with zero total orbital momentum, and the final singlet state $|\nu\mathbf{p}\rangle$ is an antisymmetrized product of the unrelaxed $1s$-bound state of the He^+ ion, $|\nu\rangle$, and the photoelectron Coulomb state, $|\mathbf{p}\rangle$, satisfying asymptotically incoming spherical wave boundary conditions [43,44]. Its multipole expansion is [see Eq. (44b) of Ref. [37]],

$$\langle \nu\mathbf{p}| = \mathcal{A}\left[\frac{1}{p} \sum_{l'm'} (-i)^{l'} e^{i\delta_{l'}} Y_{l'm'}(\hat{\mathbf{p}}) Y_{l'm'}^*(\hat{\mathbf{r}}_2) \langle \nu p l'|\mathbf{r}_1, r_2\rangle\right], \quad \text{(A16)}$$

where $\delta_{l'}$ is the l'th partial phase shift; $|\nu p l'\rangle$ is the radial part of the final-state wave function normalized on the momentum scale, so that $\langle \nu p l'|\nu p' l'\rangle = \delta(p - p')$; $\mathcal{A} = (1 + P_{12})/\sqrt{2}$ is the normalized antisymmetrization operator, where the operator P_{12} exchanges the electron coordinates $\mathbf{r}_1$ and $\mathbf{r}_2$ in order to satisfy the Pauli exclusion principle. For simplicity of notation, both below and in the main text, we use a notation for the two-electron states that denotes the quantum numbers of the active electron and suppresses those of the spectator $1s$ electron, i.e., $|\nu p l'\rangle \equiv |p l'\rangle$ and $|i\rangle \equiv |n_i 0\rangle$.

The second-order amplitude (A1) is defined as a sum over intermediate states $|q\rangle \equiv |nlm\rangle$ of the product of dipole matrix

elements,

$$T_q^{(2)} = \langle \nu \mathbf{p}|(\mathbf{e}_1 \cdot \mathbf{d})|nlm\rangle \langle nlm|(\mathbf{e}_2 \cdot \mathbf{d}')|n_i 0\rangle. \quad \text{(A17)}$$

The angular part of the matrix elements in Eq. (A17) can be easily evaluated using Eq. (A16) to obtain

$$T_q^{(2)} = \frac{\sqrt{2}}{p} \sum_{l'} \frac{(-i)^{l'} e^{i\delta_{l'}}}{\sqrt{2l'+1}} C^{l'0}_{10\,10} \left(Y_{l'}(\hat{\mathbf{p}}) \cdot \{\mathbf{e}_1 \otimes \mathbf{e}_2\}_{l'}\right) \times \langle pl'|d|n1\rangle\langle n1|d'|n_i 0\rangle. \quad \text{(A18)}$$

From the properties of the Clebsch-Gordan coefficients, it follows that $l' = 0,2$ in Eq. (A18). As a result we have

$$T_q^{(2)} = (\mathbf{e}_1 \cdot \mathbf{e}_2)\frac{1}{3\sqrt{2\pi}} \frac{e^{i\delta_0}}{p} \langle p0|d|n1\rangle\langle n1|d'|n_i 0\rangle - \frac{1}{\sqrt{\pi}} \frac{e^{i\delta_2}}{p} \left((\hat{\mathbf{p}} \cdot \mathbf{e}_1)(\hat{\mathbf{p}} \cdot \mathbf{e}_2) - \frac{1}{3}(\mathbf{e}_1 \cdot \mathbf{e}_2)\right) \times \langle p2|d|n1\rangle\langle n1|d'|n_i 0\rangle. \quad \text{(A19)}$$

The first term on the right-hand side of Eq. (A19) corresponds to a transition to a final s state of the ionized electron, while the second term corresponds to a transition to a final d state.

Thus, for the case when both photons are absorbed from the first pulse, $\mathbf{e}_2 = \mathbf{e}_1$, using Eqs. (A1) and (A19) we obtain the following structure for this term in A_2:

$$A_2(\mathbf{e}_1,\mathbf{e}_1) = e^{-2i\phi_1}\left[\mathcal{M}_d^{(1)}(\hat{\mathbf{p}} \cdot \mathbf{e}_1)^2 + \mathcal{M}_{ds}^{(1)}(\mathbf{e}_1 \cdot \mathbf{e}_1)\right], \quad \text{(A20)}$$

where $(\mathbf{e}_1 \cdot \mathbf{e}_1) \equiv \ell_1$ and the dynamical radial parameters $\mathcal{M}_s^{(1)}$ and $\mathcal{M}_d^{(1)}$, obtained after integration over both time and angular variables, are given respectively by Eqs. (12) and (9). Note that $A_2(\mathbf{e}_1,\mathbf{e}_1)$ in Eq. (A20) corresponds to Eq. (46) in Ref. [37] when emission terms are neglected. Other terms in the second-order PT amplitude [namely, $A_2(\mathbf{e}_2,\mathbf{e}_2)$, $A_2(\mathbf{e}_1,\mathbf{e}_2)$, and $A_2(\mathbf{e}_2,\mathbf{e}_1)$] can be written in a similar form. Using results similar to Eq. (A19) for the other three pathways in Eq. (A11), one arrives at the expression (7) for the second-order PT amplitude, where the parameters $\mathcal{M}_d^{(12)}(p,\tau)$ and $\mathcal{M}_{ds}^{(12)}(p,\tau)$ are given by Eqs. (15)–(17) and the parameter $\mathcal{M}_d^{(2)}$ by Eq. (14).

APPENDIX B: PROCEDURE FOR EXTRACTION OF THE DYNAMICAL PARAMETER $|\mathcal{M}_d(p)|^2$ FROM TDSE RESULTS

The PT results for the TDPs shown in Figs. 3 and 5–8 are obtained using Eqs. (24), (25), and (31), each of which depends on the squared modulus of the second-order dynamical parameter $\mathcal{M}_d(p)$. The calculation of the dynamical parameter $\mathcal{M}_d(p)$ [cf. Eq. (9)] can be carried out analytically; however, it is nontrivial as it involves Green's functions (10) and summations over the energies of intermediate states.

Instead of calculating $|\mathcal{M}_d(p)|^2$ analytically, we have determined this parameter numerically by means of *ab initio* TDSE calculations, as follows. We first solve (in the dipole approximation) the six-dimensional, two-electron TDSE for a *single* pulse that is right circularly polarized. After the end of the pulse, we project the wave packet solution of the TDSE (produced by this single pulse) onto field-free correlated multichannel scattering wave functions. The latter functions [describing the $e^- + \mathrm{He}^+(1s)$ singly ionized continuum] can be generated accurately using the so-called Jacobi- or J-matrix method [36]. In this projection, only the $L = 2, M = +2$ amplitude is included, in accord with dipole selection rules. The squared modulus of this projection equals the TDP given in Eq. (6) in which the amplitude for a single right circularly polarized pulse is given by the first term in Eq. (A20), where the geometric factor $(\hat{\mathbf{p}} \cdot \mathbf{e}_1)^2$ is given by Eq. (22). Thus, the absolute square of this projection equals $(\mathcal{C}/4)\sin^4\theta|\mathcal{M}_d(p)|^2$, where $\mathcal{C}$ is a normalization factor and $\theta = \pi/2$ for electrons detected in the polarization plane.

[1] L. de Broglie, The reinterpretation of wave mechanics, Found. Phys. **1**, 5 (1970).

[2] A. Einstein, Über einen die Erzeugung und Verwandlung des Lichtes betreffenden heuristischen Gesichtspunkt, Ann. Phys. **17**, 132 (1905).

[3] C. Davisson and L. H. Germer, Diffraction of electrons by a crystal of nickel, Phys. Rev. **30**, 705 (1927).

[4] N. F. Ramsey, A molecular beam resonance method with separated oscillating fields, Phys. Rev. **78**, 695 (1950).

[5] L. D. Noordam, D. I. Duncan, and T. F. Gallagher, Ramsey fringes in atomic Rydberg wave packets, Phys. Rev. A **45**, 4734 (1992).

[6] M. Strehle, U. Weichmann, and G. Gerber, Femtosecond time-resolved Rydberg wave-packet dynamics in the two-electron system calcium, Phys. Rev. A **58**, 450 (1998).

[7] M. Wollenhaupt, A. Assion, D. Liese, Ch. Sarpe-Tudoran, T. Baumert, S. Zamith, M. A. Bouchene, B. Girard, A. Flettner, U. Weichmann, and G. Gerber, Interferences of Ultrashort Free Electron Wave Packets, Phys. Rev. Lett. **89**, 173001 (2002).

[8] J. M. Ngoko Djiokap, S. X. Hu, L. B. Madsen, N. L. Manakov, A. V. Meremianin, and A. F. Starace, Electron Vortices in Photoionization by Circularly Polarized Attosecond Pulses, Phys. Rev. Lett. **115**, 113004 (2015).

[9] M. Harris, C. A. Hill, and J. M. Vaughan, Optical helices and spiral interference fringes, Opt. Commun. **106**, 161 (1994).

[10] C. A. Mancuso, D. D. Hickstein, P. Grychtol, R. Knut, O. Kfir, X.-M. Tong, F. Dollar, D. Zusin, M. Gopalakrishnan, C. Gentry, E. Turgut, J. L. Ellis, M.-C. Chen, A. Fleischer, O. Cohen, H. C. Kapteyn, and M. M. Murnane, Strong-field ionization with two-color circularly polarized laser fields, Phys. Rev. A **91**, 031402(R) (2015).

[11] N. Douguet, A. N. Grum-Grzhimailo, E. V. Gryzlova, E. I. Staroselskaya, J. Venzke, and K. Bartschat, Photoelectron angular distributions in bichromatic atomic ionization induced by circularly polarized VUV femtosecond pulses, Phys. Rev. A **93**, 033402 (2016).

[12] I. Bialynicki-Birula, Z. Bialynicka-Birula, and C. Sliwa, Motion of vortex lines in quantum mechanics, Phys. Rev. A **61**, 032110 (2000).

[13] S. J. Ward and J. H. Macek, Effect of a vortex in the triply differential cross section for electron-impact K-shell ionization of carbon, Phys. Rev. A **90**, 062709 (2014).

[14] J. H. Macek, J. B. Sternberg, S. Y. Ovchinnikov, and J. S. Briggs, Theory of Deep Minima in $(e,2e)$ Measurements of Triply Differential Cross Sections, Phys. Rev. Lett. **104**, 033201 (2010).

[15] J. M. Feagin, Vortex kinematics of a continuum electron pair, J. Phys. B **44**, 011001 (2011).

[16] J. H. Macek, J. B. Sternberg, S. Y. Ovchinnikov, T.-G. Lee, and D. R. Schultz, Origin, Evolution, and Imaging of Vortices in Atomic Processes, Phys. Rev. Lett. **102**, 143201 (2009).

[17] F. Navarrete, R. Della Picca, J. Fiol, and R. O. Barrachina, Vortices in ionization collisions by positron impact, J. Phys. B **46**, 115203 (2013).

[18] L. Ph. H. Schmidt, C. Goihl, D. Metz, H. Schmidt-Böcking, R. Dörner, S. Yu. Ovchinnikov, J. H. Macek, and D. R. Schultz, Vortices Associated with the Wave Function of a Single Electron Emitted in Slow Ion-Atom Collisions, Phys. Rev. Lett. **112**, 083201 (2014).

[19] S. Y. Ovchinnikov, J. H. Macek, and D. R. Schultz, Hydrodynamical interpretation of angular momentum and energy transfer in atomic processes, Phys. Rev. A **90**, 062713 (2014).

[20] S. Y. Ovchinnikov, J. B. Sternberg, J. H. Macek, T.-G. Lee, and D. R. Schultz, Creating and Manipulating Vortices in Atomic Wave Functions with Short Electric Field Pulses, Phys. Rev. Lett. **105**, 203005 (2010).

[21] J. Feist, S. Nagele, C. Ticknor, B. I. Schneider, L. A. Collins, and J. Burgdörfer, Attosecond Two-Photon Interferometry for Doubly Excited States of Helium, Phys. Rev. Lett. **107**, 093005 (2011).

[22] W.-C. Jiang, W.-H. Xiong, T.-S. Zhu, L.-Y. Peng, and Q. Gong, Double ionization of He by time-delayed attosecond pulses, J. Phys. B **47**, 091001 (2014).

[23] A. N. Grum-Grzhimailo, E. V. Gryzlova, E. I. Staroselskaya, J. Venzke, and K. Bartschat, Interfering one-photon and two-photon ionization by femtosecond VUV pulses in the region of an intermediate resonance, Phys. Rev. A **91**, 063418 (2015).

[24] J. M. Ngoko Djiokap, N. L. Manakov, A. V. Meremianin, S. X. Hu, L. B. Madsen, and A. F. Starace, Nonlinear Dichroism in Back-to-Back Double Ionization of He by an Intense Elliptically Polarized Few-Cycle Extreme Ultraviolet Pulse, Phys. Rev. Lett. **113**, 223002 (2014).

[25] M. S. Pindzola and F. Robicheaux, Total ionization cross section for electron-hydrogen scattering using a time-dependent close-coupling method, Phys. Rev. A **54**, 2142 (1996).

[26] M. S. Pindzola and F. Robicheaux, Time-dependent close-coupling calculations of correlated photoionization processes in helium, Phys. Rev. A **57**, 318 (1998).

[27] H. G. Muller, An efficient propagation scheme for the time-dependent Schrödinger equation in the velocity gauge, Laser Phys. **9**, 138 (1999).

[28] T. K. Kjeldsen, L. A. A. Nikolopoulos, and L. B. Madsen, Solving the m-mixing problem for the three-dimensional time-dependent Schrödinger equation by rotations: Application to strong-field ionization of H_2^+, Phys. Rev. A **75**, 063427 (2007).

[29] C. P. J. Martiny, M. Abu-samha, and L. B. Madsen, Counterintuitive angular shifts in the photoelectron momentum distribution for atoms in strong few-cycle circularly polarized laser pulses, J. Phys. B **42**, 161001 (2009).

[30] C. P. J. Martiny, M. Abu-samha, and L. B. Madsen, Ionization of oriented targets by intense circularly polarized laser pulses: Imprints of orbital angular nodes in the two-dimensional momentum distribution, Phys. Rev. A **81**, 063418 (2010).

[31] M. Abu-samha and L. B. Madsen, Interrogation of orbital structure by elliptically polarized intense femtosecond laser pulses, Phys. Rev. A **84**, 023411 (2011).

[32] A. N. Pfeiffer, C. Cirelli, M. Smolarski, D. Dimitrovski, M. Abu-samha, L. B. Madsen, and U. Keller, Attoclock reveals natural coordinates of the laser-induced tunneling current flow in atoms, Nat. Phys. **8**, 76 (2012).

[33] N. I. Shvetsov-Shilovski, D. Dimitrovski, and L. B. Madsen, Ehrenfest's theorem and the validity of the two-step model for strong-field ionization, Phys. Rev. A **87**, 013427 (2013).

[34] S. X. Hu, Optimizing the FEDVR-TDCC code for exploring the quantum dynamics of two-electron systems in intense laser pulses, Phys. Rev. E **81**, 056705 (2010).

[35] L. B. Madsen, L. A. A. Nikolopoulos, T. K. Kjeldsen, and J. Fernández, Extracting continuum information from $\Psi(t)$ in time-dependent wave-packet calculations, Phys. Rev. A **76**, 063407 (2007).

[36] J. M. Ngoko Djiokap, S. X. Hu, W.-C. Jiang, L.-Y. Peng, and A. F. Starace, Enhanced asymmetry in few-cycle attosecond pulse ionization of He in the vicinity of autoionizing resonances, New J. Phys. **14**, 095010 (2012).

[37] E. A. Pronin, A. F. Starace, M. V. Frolov, and N. L. Manakov, Perturbation theory analysis of attosecond photoionization, Phys. Rev. A **80**, 063403 (2009).

[38] O. Kfir, P. Grychtol, E. Turgut, R. Knut, D. Zusin, D. Popmintchev, T. Popmintchev, H. Nembach, J. M. Shaw, A. Fleischer, H. Kapteyn, M. Murnane, and O. Cohen, Generation of bright phase-matched circularly polarized extreme ultraviolet high harmonics, Nat. Photon. **9**, 99 (2014).

[39] Gy. Tóth, Z. Tibai, Zs. Nagy-Csiha, Zs. Márton, G. Almási, and J. Hebling, Circularly Polarized Carrier-Envelope-Phase-Stable Attosecond Pulse Generation based on coherent undulator radiation, Opt. Lett. **40**, 4317 (2015).

[40] L. Medišauskas, J. Wragg, H. van der Hart, and M. Yu. Ivanov, Generating Isolated Elliptically Polarized Attosecond Pulses Using Bichromatic Counterrotating Circularly Polarized Laser Fields, Phys. Rev. Lett. **115**, 153001 (2015).

[41] D. M. Reich and L. B. Madsen, A rotating-frame perspective on high-harmonic generation of circularly polarized light, Phys. Rev. A **93**, 043411 (2016).

[42] A. S. Davydov, *Quantum Mechanics*, 2nd ed. (Pergamon, Oxford, 1965).

[43] A. F. Starace, *Theory of Atomic Photoionization*, Handbuch der Physik, edited by W. Mehlhorn (Springer-Verlag, Berlin, 1982), Vol. 31, pp. 1–121.

[44] L. D. Landau and E. M. Lifshitz, *Quantum Mechanics: Non-Relativistic Theory*, 3rd ed. (Pergamon, Oxford, 1977).

[45] K.-J. Yuan, S. Chelkowski, and A. D. Bandrauk, Photoelectron momentum distributions of molecules in bichromatic circularly polarized attosecond UV laser fields, Phys. Rev. A **93**, 053425 (2016).